# Modelling cell movement, cell differentiation, cell sorting and proportion regulation in Dictyostelium discoideum aggregations

Pineda, M.; Weijer, C. J.; Eftimie, R.

*Published in:*
Journal of Theoretical Biology

*DOI:*
10.1016/j.jtbi.2015.01.042

*Publication date:*
2015

Modelling cell movement, cell differentiation, cell sorting and proportion regulation in Dictyostelium discoideum aggregations

M. Pinedaa, , , C.J. Weijerb, , R. Eftimiea,
published in Journal of Theoretical Biology, Volume 370, 7 April 2015, Pages 135–150

# Modelling cell movement, cell differentiation, cell sorting and proportion regulation in *Dictyostelium discoideum* aggregations

M. Pineda[a], C. J. Weijer[b], R. Eftimie[a,*]

[a] *Division of Mathematics, University of Dundee, Dundee, United Kingdom, DD1 4HN*
[b] *School of Life Sciences, University of Dundee, Dundee, United Kingdom, DD1 4HN*

**Abstract**

Understanding the mechanisms that control tissue morphogenesis and homeostasis is a central goal not only in developmental biology but also has great relevance for our understanding of various diseases, including cancer. A model organism that is widely used to study the control of tissue morphogenesis and proportioning is the *Dictyostelium discoideum*. While there are mathematical models describing the role of chemotactic cell motility in the *Dictyostelium* assembly and morphogenesis of multicellular tissues, as well as models addressing possible mechanisms of proportion regulation, there are no models incorporating both these key aspects of development. In this paper, we introduce a 1D hyperbolic model to investigate the role of two morphogens, DIF and cAMP, on cell movement, cell sorting, cell-type differentiation and proportioning in *Dictysotelium discoideum*. First, we use the non-spatial version of the model to study cell-type transdifferentiation. We perform a steady-state analysis of it and show that, depending on the shape of the differentiation rate functions, multiple steady-state solutions may occur. Then we incorporate spatial dynamics into the model, and investigate the transdifferentiation and spatial positioning of cells inside the newly formed structures, following the removal of prestalk or prespore regions of a *Dictyostelium* slug. We show that in isolated prespore fragments, a tipped mound-like aggregate can be formed after a transdifferentiation from pres-

*Corresponding author.
Phone: +44 (0)1382 384488; Fax: +44 (0)1382 385516
*Email addresses:* mpineda@maths.dundee.ac.uk (M. Pineda), c.j.weijer@dundee.ac.uk (C. J. Weijer), reftimie@maths.dundee.ac.uk (R. Eftimie)

pore to prestalk cells and following the sorting of prestalk cells to the centre of the aggregate. For isolated prestalk fragments, we show the formation of a slug-like structure containing the usual anterior-posterior pattern of prestalk and prespore cells.

*Keywords:* cell-type differentiation, collective cell movement, *Dictyostelium discoideum*, negative signalling feedback

---

## 1. Introduction

A major goal in developmental studies is to understand the relationship between cell movement and cell differentiation. The genetically tractable social amoebae *Dictyostelium discoideum* is one of the simplest model organisms suited to study this problem [1, 2, 3, 4]. In the development of *Dictyostelium*, a multicellular mound is formed by the aggregation of a large number of amoebae which have ceased to feed [5, 7, 8]. Upon mound formation, cells start to differentiate and form a salt-and-pepper (random) distribution of prespore (PSP) and prestalk (PST) cells inside the mound (see Fig. 1(a)). Then, a subpopulation of PST cells sort out to form the tip, and the mound elongates to become a cylindrical finger that falls onto the substratum and forms the migrating slug. After the slug migrates for a period of time, it rises into the air and forms a fruiting body consisting of stalk and spore cells. Under favourable conditions the spores can germinate to release amoebae again. In regard to the structure of the migrating slugs, it is known that the PST cells occupy approximately the anterior 20% of the slug, while the rear part of the slug contains PSP cells intermingled with a type of PST cells known as anterior-like cells (ALC) (See Fig. 1 (b)) [9, 10]. This distribution of cell types is relatively constant for slugs of different sizes [11]. Moreover, a few studies show that when a slug is cut into two pieces, separating the prestalk and prespore zones, both pieces can partially or fully restore a normally-patterned slug with correct cell proportioning by inducing cell-type conversion and cell sorting [12, 13]. However, there are also few experimental reports suggesting that proportions are not exactly restored in slugs after one cell type is removed [9]. While the signalling pathways involved in all these individual aspects of *Disctyostelium* aggregations (i.e., differentiation, proportioning, migration and sorting) have been studied intensively over the past years, it is still not very clear how they interact with each other to control in a unitary manner these aggregations.

The purpose of this work is to present and analyse a mathematical model that can qualitatively reproduce the phenomena of cell movement, cell sorting and proportion regulation occurring in slug amputation experiments.

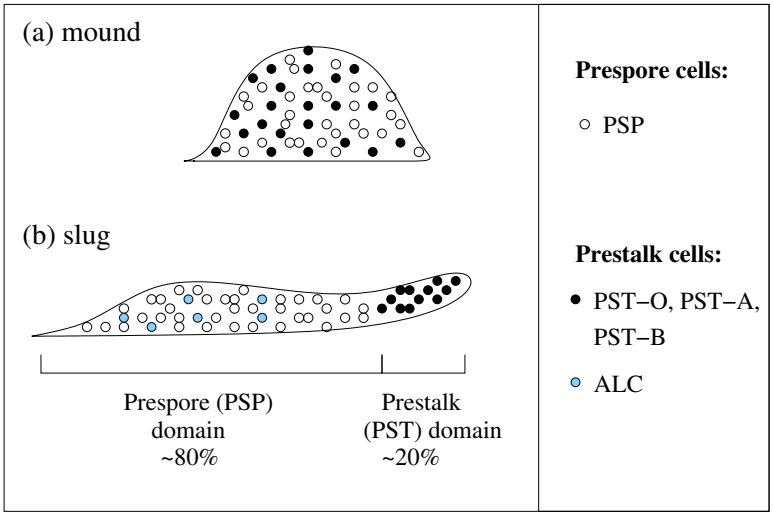


Figure 1: (a) Simplified description of cell distribution inside the mound. (b) Simplified description of cell distribution and proportioning in the slug. PSP=prespore cells; ALC=anterior-like cells (a prestalk-type cell population); PST-A, PST-B, PST-O=prestalk cell types. The tip of the slug (i.e., prestalk domain) has two main regions: an anterior region formed of PST-A cells and a posterior region formed of PST-O cells. A third type of PST cell, namely PST-B, can be found at the core of the tip.

Over the last two decades, mathematical models (of continuous and discrete type, or a combination of the two) have been derived to analyse various aspects of *Dictyostelium discoideum* morphogenesis [14, 15, 16, 17, 18, 19, 20, 21, 22]. For example, it has been shown that the aggregation of single cells is driven mainly by chemotaxis to cyclic adenosine-3',5'-monophosphate (cAMP) [14, 15, 16]. Other studies on mound formation and slug motion emphasised also the importance of mechanical interactions between cells [16, 17, 18, 19, 20, 21, 22]. Models aimed to describe the process of culmination in *Dictyostelium discoideum* showed that cAMP signalling and mechanical interactions, combined with cell differentiation, are sufficient to produce the cell movements which lead to the formation of the fruiting body [23]. There are also a few studies who consider the role of feedback signalling mechanisms on cell proportioning inside stationary *Dictyostelium* aggrega-

tions [24, 25, 26, 27]. However, none of these studies investigate in an unitary manner the role of various signalling mechanisms on cell-type proportioning, cell sorting, cell migration and cell aggregation.

The main goal of this study is to investigate the interplay between two signalling factors, cAMP and the so-called differentiation-induced factor (DIF), on the following aspects of stationary and moving *Dictyostelium* aggregations: (i) cell differentiation and proportioning; (ii) spatial sorting of prespore and prestalk cells inside these aggregations. To this end, we introduce two mathematical models: a *non-spatial model* that is used to investigate the signalling mechanisms that control cell-type proportioning, and a *nonlocal spatial model* that is used to investigate the role of these signalling mechanisms on cell movement and cell spatial sorting inside aggregations. In particular, we use these models to reproduce the regeneration and cell-sorting phenomena that occur after the removal of different parts of *Dictyostelium* slugs [9, 10, 12, 13].

The article is structured as follows. In Section 2, we introduce the biological mechanism for cell-type proportioning of *Dictyostelium* cells. In Section 3, we introduce a non-spatial mathematical model that incorporates this biological mechanism. We also present here an analysis of the steady states of the model. In Section 4 we generalise the non-spatial model to include also spatial interactions between cells (via nonlocal mechanical forces and chemical signalling). The problem of pattern formation through cell sorting is analysed. Summary and discussions of the results are presented in Section 5.

## 2. Signalling mechanisms involved in cell-type differentiation and cell proportioning

Experimental studies have shown that the differentiation of *Dictyostelium* cells into prestalk and prespore cells and the regulation of proportions between these two types of cells is controlled by two main morphogens: cAMP and DIF [3, 4]. In particular, it has been shown that:

- DIF is predominantly made by prespore cells and degraded by prestalk cells [4, 28];
- DIF signalling induces differentiation of prestalk cells and blocks prespore differentiation by inhibiting cAMP signalling [4, 28, 29, 30];

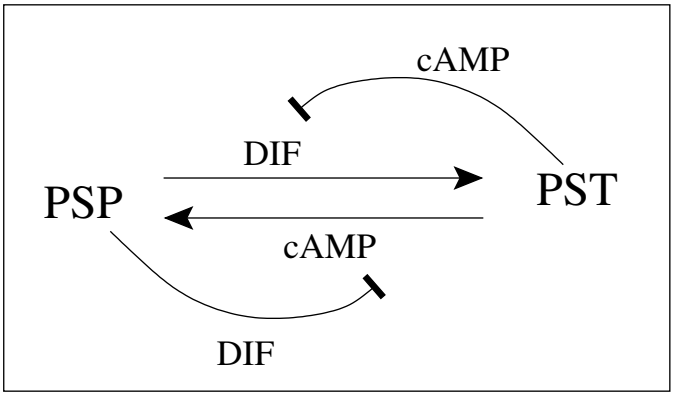


Figure 2: Schematic representation of the cAMP and DIF signalling pathways behind cell differentiation (PST→PSP and PSP→PST) and cell proportioning. These mechanisms, which have been proposed in [1, 3], are modelled in Section 3.

- cAMP is predominantly made by prestalk cells and anterior-like cells and degraded by prespore cells [31, 32, 33];
- cAMP signalling induces prespore cell differentiation and blocks prestalk cell differentiation by inhibiting DIF signalling [31, 32, 33].

These biological assumptions are summarised schematically in Figure 2. In the following section, we present a mathematical model for cell differentiation and cell proportioning, which incorporates these mechanisms.

## 3. Non-spatial model

Throughout this section, we ignore the spatial movement of cells and spatial distribution of chemicals, and introduce a non-spatial mathematical model that describes the mechanism presented in Figure 2 [**?** **?** ]. We then use this model to analyse several aspects of cell-type conversion and proportioning inside intact slugs (where the PST:PSP cell proportions are ≈20:80) and inside slugs formed of various proportions of PST and PSP cells (i.e., with PST:PSP proportions ranging from 0:100 to 100:0).

Let us denote the total number of PSP and PST cells inside the aggregate by $U_P$ and $U_T$, respectively. We also denote the concentration of cAMP by $v_c$ and the concentration of DIF by $v_D$ (see also Table B.1). The non-spatial

equations describing the mechanism presented in Figure 2 are:

$$\frac{dU_P}{dt} = -k_1 g_1(v_D) f_2(v_c) U_P + k_2 g_2(v_D) f_1(v_c) U_T, \tag{1a}$$

$$\frac{dU_T}{dt} = k_1 g_1(v_D) f_2(v_c) U_P - k_2 g_2(v_D) f_1(v_c) U_T, \tag{1b}$$

$$\frac{dv_D}{dt} = p_1 U_P - d_1 v_D U_T, \tag{1c}$$

$$\frac{dv_c}{dt} = p_2 U_T - d_2 v_c U_P. \tag{1d}$$

Here $k_1$ and $k_2$ describe the transition rates for the PSP $\rightarrow$ PST and PST $\rightarrow$ PSP differentiation, respectively. Functions $f_1$, $g_1$ and $f_2$, $g_2$ describe the positive and negative feedback effects of cAMP and DIF on these transitions. Since experimental studies suggested a cAMP and DIF concentration-dependent induction of prestalk and prespore markers [28, 30, 32], we choose Hill-type forms for these transition functions (for examples of other types of transition functions see Remarks 1 and 2):

$$g_1(v_D) = \frac{v_D^{n_d}}{a_0^{n_d} + v_D^{n_d}}, \quad f_2(v_c) = \frac{b_1^{n_c}}{b_1^{n_c} + v_c^{n_c}}, \tag{2a}$$

$$g_2(v_D) = \frac{b_0^{n_d}}{b_0^{n_d} + v_D^{n_d}}, \quad f_1(v_c) = \frac{v_c^{n_c}}{a_1^{n_c} + v_c^{n_c}}. \tag{2b}$$

Here, $b_0$ and $a_1$ denote the half-maximum concentrations for DIF and cAMP that control the transition PST $\rightarrow$ PSP. Similarly, $a_0$ and $b_1$ denote the half-maximum concentrations for DIF and cAMP controlling the transition PSP $\rightarrow$ PST. Functions $g_1(v_D)$ and $f_1(v_c)$ are increasing saturation functions of signalling chemicals, implying that $v_D$ and $v_c$ promote PSP $\rightarrow$ PST and PST $\rightarrow$ PSP conversions, respectively. Because these transitions can also be suppressed by these two signalling chemicals, $g_2(v_c)$ and $f_2(v_D)$ are decreasing functions of $v_c$ and $v_D$, respectively. The coefficients $n_d$ and $n_c$ that appear in (2) control the steepness of the functions: large exponents model very abrupt responses to the chemicals' concentrations, while small exponents model smoother responses to these concentrations. We will come back to these saturation functions in Section 3.1, when we will discuss their role on preserving the correct PSP:PST proportions.

Finally, in Eqs. (1c) and (1d), $p_1$ and $p_2$ are the production rates of DIF and cAMP by the PSP and PST cells, respectively. Similarly, $d_1 v_D$ and $d_2 v_c$

are the degradation rates of DIF and cAMP, in the presence of PST and PSP cells, respectively.

### *3.1. Steady states and the shape of saturation functions*

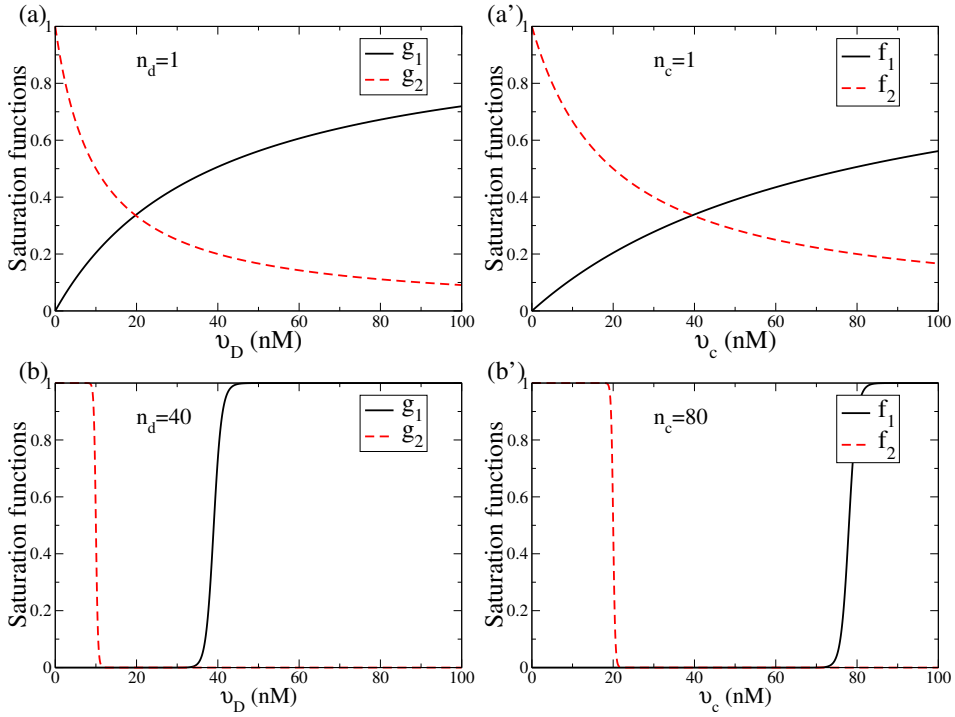


Figure 3: Examples of saturation functions in (2) for different values of the exponent coefficients: (a)-(a') $n_d = n_c = 1$ and (b)-(b') $n_d = 40, n_c = 80$. Left panels show saturation functions $g_1(v_D)$ and $g_2(v_D)$. Right panels show saturation functions $f_1(v_c)$ and $f_2(v_c)$. Half maxima concentrations for the saturation functions are $a_0 = 39$ nM, $b_0 = 10$ nM, $b_1 = 20$ nM, and $a_1 = 77$ nM.

There are a few experimental reports claiming that the final proportion of PST:PSP cells is not always exactly 20:80, but varies around this value. For example, in [9] it was showed that the ratio PST:PSP can be anywhere between 10:90 and 30:70. In the following, we investigate a possible phenomenological mechanism that could explain the existence of steady states with PST and PSP cells in various proportions. To this end, we focus on the exponents $n_c$ and $n_d$ that appear in equations (2). Varying these exponents

leads to changes in the steepness of functions $f_{1,2}$ and $g_{1,2}$, as shown in Figure 3. We note in panels (b) and (b') that for very steep functions, there are certain ranges for the concentration of DIF ($v_D \in (12, 35)$) and cAMP ($v_c \in (22, 72)$) for which $f_{1,2}, g_{1,2} \approx 0$. Therefore, in this case, any $U_P$ and $U_T$ can be solutions for equations (1a)-(1b). The exact values of these solutions can be obtained from equations (1c)-(1d), where parameters can be chosen such that the ratio PSP:PST is between 10:90 and 30:70.

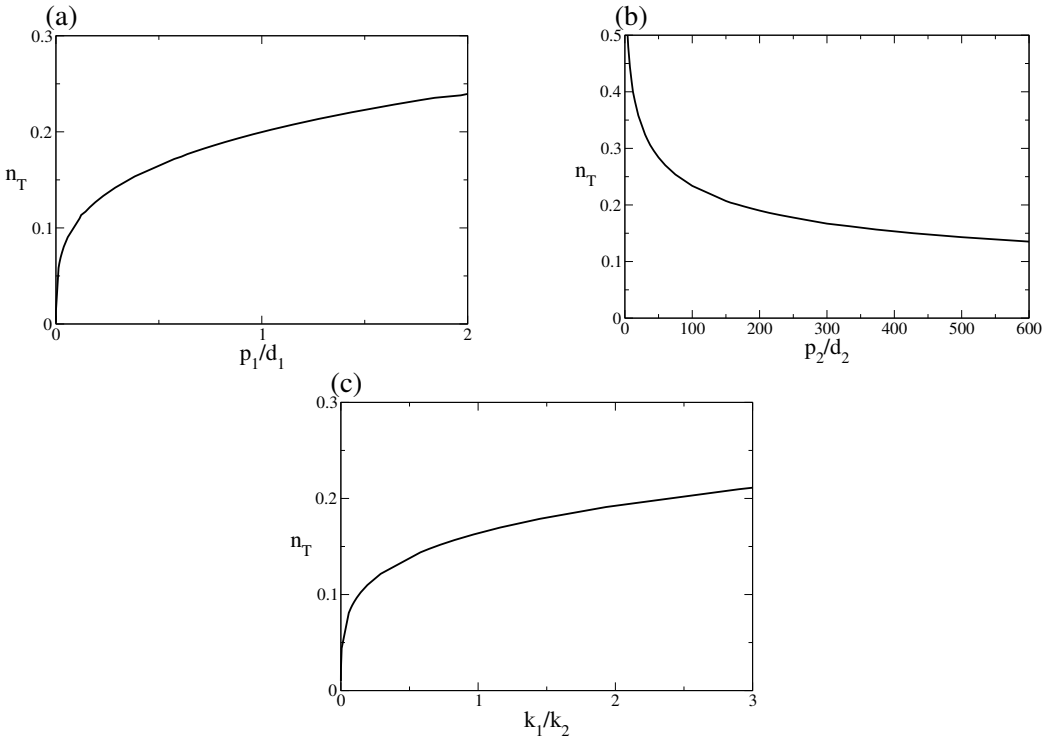


Figure 4: The steady state for the proportion $n_T$ of PST cells (see equation (**??**)) as a function of different model parameters: (a) $p_1/d_1$, (b) $p_2/d_2$, and (c) $k_1/k_2$. Here we show only the case $n_c = n_d = 1$. The parameters are: (a) $k_1 = 0.58$ h$^{-1}$, $k_2 = 0.26$ h$^{-1}$, $p_2 = 3.0$ nM h$^{-1}$, $d_2 = 0.017$ h$^{-1}$; (b) $p_1 = 0.115$ nM h$^{-1}$, $d_1 = 0.12$ h$^{-1}$, $k_1 = 0.58$ h$^{-1}$, $k_2 = 0.26$ h$^{-1}$; (c) $p_1 = 0.115$ nM h$^{-1}$, $d_1 = 0.12$ h$^{-1}$, $p_2 = 3.0$ nM h$^{-1}$, $d_2 = 0.017$ h$^{-1}$. The rest of parameters are: $a_0 = 39$ nM, $b_0 = 10$ nM, $b_1 = 20$ nM, $a_1 = 77$ nM.

Next, we investigate in more detail the number of the steady states of model (1), for small and large values of $n_c$ and $n_d$:

(I) For small $n_c$ and $n_d$ values, there are positive intersection points between functions $g_1$ and $g_2$, and between $f_1$ and $f_2$ (as for the case

$n_d = n_c = 1$ shown in Fig. 3(a),(a')). In this case, there is only one steady state solution $(U_P, U_T, v_D, v_c)$. Since some experimental papers present their results in terms of the proportion of prestalk cells in the *Dictyosteium* aggregations [9], we decided to calculate this steady state in terms of the final PST proportion:

$$n_T = \frac{U_T}{U_T + U_P}. \tag{3}$$

For simplicity, in the following we focus only on the case $n_d = n_c = 1$. Then, $n_T$ is the solution of

$$\frac{(1-n_T)}{n_T}\left(\frac{b_1 k_1 p_1}{d_1}\right)\left(b_0 + \frac{p_1}{d_1}\frac{(1-n_T)}{n_T}\right)\left(a_1\frac{(1-n_T)}{n_T} + \frac{p_2}{d_2}\right)$$
$$-\left(\frac{k_2 b_0 p_2}{d_2}\right)\left(b_1 + \frac{p_2}{d_2}\frac{n_T}{(1-n_T)}\right)\left(a_0\frac{n_T}{(1-n_T)} + \frac{p_1}{d_1}\right) = 0. \tag{4}$$

A detailed derivation of this equation is presented in Appendix C. Because the total number of cells is conserved (see equations (1)), the steady state for the proportion of PSP cells is given by $n_P = 1 - n_T$. The steady states for $v_c$ and $v_D$ are given by

$$v_c = \frac{n_T p_2}{d_2(1-n_T)}, \quad v_D = \frac{p_1(1-n_T)}{n_T d_1}. \tag{5}$$

Since it is impossible to write down a closed-form equation for $n_T$, we plot in Fig. 4 this proportion as a function of various model parameters: (a) $n_T$ versus $p_1/d_1$, (b) $n_T$ versus $p_2/d_2$, and (c) $n_T$ versus $k_1/k_2$. Finally, to check that the long-term dynamics of model (1) indeed approaches theses steady states, we fix the model parameters such that $n_T = 0.2$ in (4). We show in Fig. 5 that for different initial conditions $n_T(0)$, the solution trajectories of (1) do approach $n_T = 0.2$, as expected.

(II) For large $n_c$ and $n_d$ values, there are no positive intersection points between $g_1$ and $g_2$ or between $f_1$ and $f_2$ (see Fig. 3(b),(b')), and in this case it is possible to have multiple steady state solutions $(U_P, U_T, v_D, v_c)$ for system (1). These solutions are related to the final equilibrium PST proportion as follows:

$$n_T = \frac{U_T}{U_T + U_P} = \frac{p_1}{p_1 + d_1 v_d} = \frac{d_2 v_c}{p_2 + d_2 v_c}. \tag{6}$$

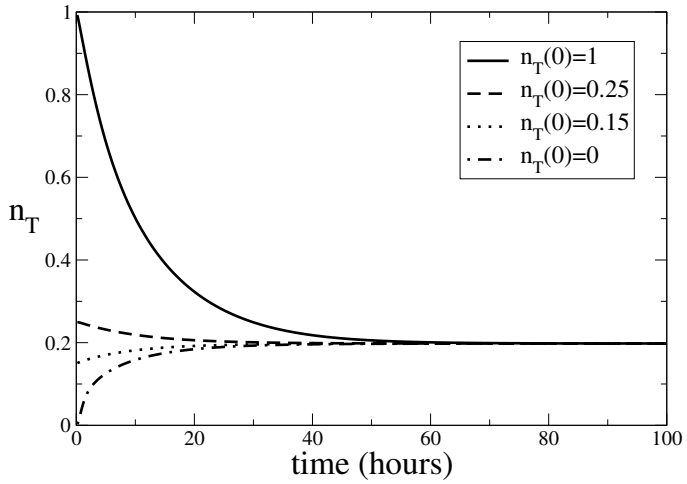


Figure 5: The proportion of PST cells, $n_T$, as a function of time, for different initial conditions $n_T(0)$. Here we show only the case $n_c = n_d = 1$. The parameters are: $a_0 = 39$ nM, $b_0 = 10$ nM, $b_1 = 20$ nM, and $a_1 = 77$ nM, $k_1 = 0.58$ h$^{-1}$, $k_2 = 0.26$ h$^{-1}$, $p_1 = 0.115$ nM h$^{-1}$, $d_1 = 0.12$ h$^{-1}$, $p_2 = 3.0$ nM h$^{-1}$, $d_2 = 0.017$ h$^{-1}$. The initial conditions for chemical signals are: $v_c(0) = v_D(0) = 0$ nM. The total number of cells is $U_T + U_P = 1000$.

For simplicity, we focus on the case $n_c, n_d \to \infty$, which leads to step-like functions for $f_{1,2}$ and $g_{1,2}$. This allows us to approximate the half-maxima concentrations of cAMP and DIF as the the maximum and minimum values between which there is an infinite number of steady-state solutions (see also Fig. 3(b),(b'), with $b_0 = 10$, $a_0 = 39$, $b_1 = 20$, $a_1 = 77$):

$$b_0 < v_D < a_0, \quad b_1 < v_c < a_1.$$

For these concentration values, the steady states $n_T$ satisfy $n_T^{min} < n_T < n_T^{max}$, with

$$n_T^{min} = \frac{p_1}{p_1 + d_1 a_0}, \quad n_T^{max} = \frac{p_1}{p_1 + d_1 b_0}, \tag{7}$$

or

$$n_T^{min} = \frac{d_2 b_1}{p_2 + d_2 b_1}, \quad n_T^{max} = \frac{d_2 a_1}{p_2 + d_2 a_1}, \tag{8}$$

as given by equations (1c) or (1d). After simple algebra, one obtains:

$$a_1 = \frac{n_T^{max}(1 - n_T^{min})}{n_T^{min}(1 - n_T^{max})} b_1, \quad a_0 = \frac{n_T^{max}(1 - n_T^{min})}{n_T^{min}(1 - n_T^{max})} b_0. \tag{9}$$

The parameters involved in these equations can be taken from exper-

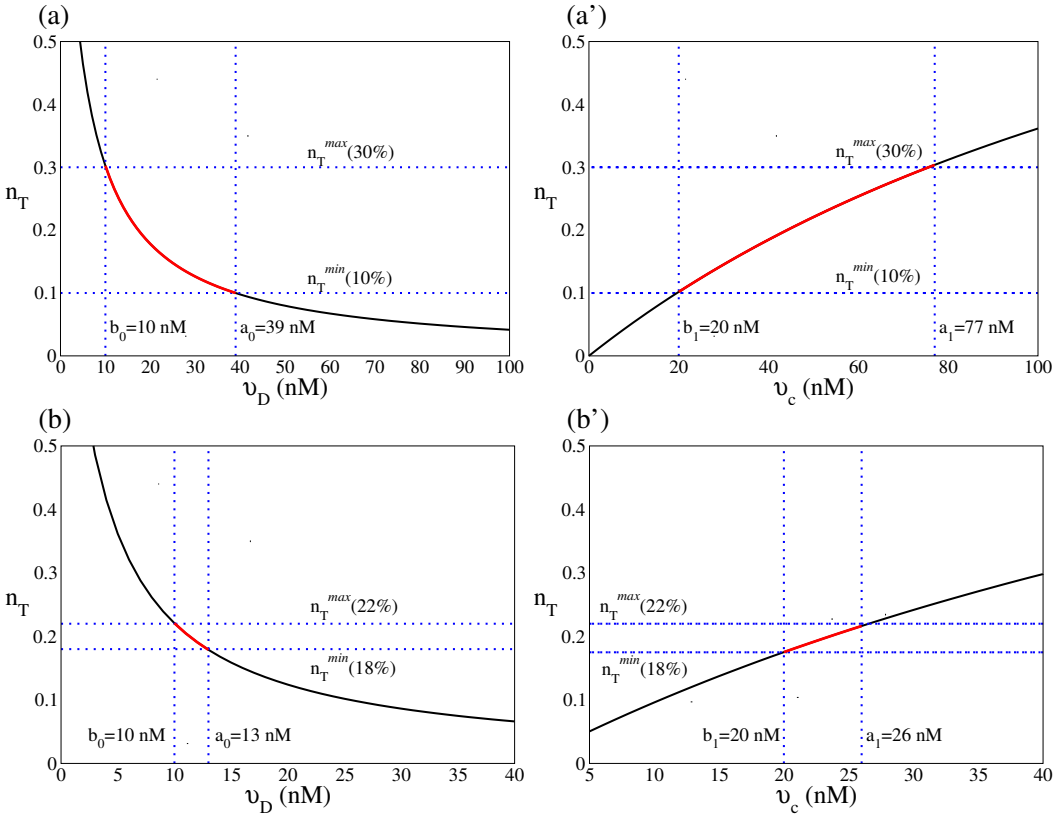


Figure 6: Consider the situation when $n_c, n_d \to \infty$. In (a), (a') we consider $n_T^{max} = 0.3$ and $n_T^{min} = 0.1$, and graph $n_T$ versus $v_D$ (panel (a)) and $n_T$ versus $v_c$ (panel (a')). For this case, the parameters are: $a_0 = 39$ nM, $b_0 = 10$ nM, $b_1 = 20$ nM, $a_1 = 77$ nM, $p_1 = 0.52$ nM h$^{-1}$, $d_1 = 0.12$ h$^{-1}$, $p_2 = 3.0$ nM h$^{-1}$, $d_2 = 0.017$ h$^{-1}$. In (b), (b') we consider $n_T^{max} = 0.22$ and $n_T^{min} = 0.18$, and again graph $n_T$ versus $v_D$ (panel (b)) and $n_T$ versus $v_c$ (panel (b')). For this case, the parameters are: $a_0 = 13$ nM, $b_0 = 10$ nM, $b_1 = 20$ nM, $a_1 = 26$ nM, $p_1 = 0.34$ nM h$^{-1}$ and $d_1 = 0.12$ h$^{-1}$, $p_2 = 1.6$ nM h$^{-1}$, $d_2 = 0.017$ h$^{-1}$. Note that the whole set of fixed points inside the squares are possible solutions, provided the saturation functions are sharp enough.

iments. For example, an experimental report in [9] showed that the proportion of prestalk cells in the slug can be anywhere between 10% and 30%, which gives us $n_T^{min} = 0.1$ and $n_T^{max} = 0.3$. Other studies suggest a less variation in the prestalk proportion [11, 12]. Using this

information, together with the experimentally-reported half-maxima concentrations for cAMP and DIF that inhibit cell differentiation (see [30]), we can calculate $a_0$ and $a_1$.

In Fig. 6, we use relations (7)-(9) to construct the phase-plane diagrams showing the steady states $n_T$ versus $v_D$ or $v_c$. The red (i.e., gray on black/white prints) curves represent the set of all possible solutions $n_T$. Ràfols et al. [27] showed similar results in a model that incorporated unrealistic transdifferentiation rates (since the rates were not taking into account realistic saturation thresholds for cell transdifferentiation that were observed experimentally) and a negative feedback mechanism for cell-type proportioning mediated only by DIF.

As mentioned above, experimental studies have also shown that the removal of different parts of the slug (i.e., the whole prestalk region or the whole prespore region) leads to cell de-differentiation to either the initial PST:PSP ratio of 20:80, or to ratios of PST:PSP varying between 10:90 and 30:70. We investigate this aspect further in Fig. 7, where we graph the time-evolution of $n_T$ for different initial conditions corresponding to different cuts of the slug: $n_T(0) = 0$ means that the whole prestalk region of the slug is removed; $n_T(0) = 1$ means that the whole prespore region of the slug is removed; $n_T(0) = 0.2$ means that the slug is intact. Panels (a)-(a') correspond to $n_T^{min} = 0.1$ and $n_T^{max} = 0.3$, while panels (b)-(b') correspond to $n_T^{min} = 0.18$ and $n_T^{max} = 0.22$, for different values of $n_c$ and $n_d$. First, let us focus on panels (a)-(a'). We notice in Fig. 7(a) that for large $n_c$ and $n_d$, the final $n_T$ proportions depend on the initial conditions: for $n_T(0) = 1$ then $n_T(\infty) \approx n_T^{max}$; for $n_T(0) = 0$ then $n_T(\infty) \approx n_T^{min}$; for $n_T(0) = 0.2$, then $n_T(\infty) = 0.2$. The reason for this behaviour is that once the solution $n_T$ enters the region $(n_T^{min}, n_T^{max})$, there is no more differentiation and $n_T$ does not change. If the solution starts inside this regions, as is the case for $n_T = 0.2$, because there is no differentiation, it will keep its initial value. As we decrease $n_c$ and $n_d$, we observe that the solution $n_T$ approaches $n_T(\infty) = 0.2$. To discuss the dynamics observed in panels (b)-(b'), we first need to specify that for this case, because $n_T^{min} = 0.18$ and $n_T^{max} = 0.22$, the half-maxima concentration values for $a_0$ and $a_1$ (as given by Eq. (9)) are slightly different from the values in Fig. 3 (see also caption for Fig. 6(b),(b')). This leads to functions $f_{1,2}$ and $g_{1,2}$ that have positive intersection points (see Fig. A.14 in Appendix A), which causes de-differentiation between the PSP and PST cells

even after the solution curves entered the region $(n_T^{min}, n_T^{max})$. For this reason, in Fig. 7(b'), if we start within this region (i.e., $n_T(0) = 0.2$), the solution still changes in time.

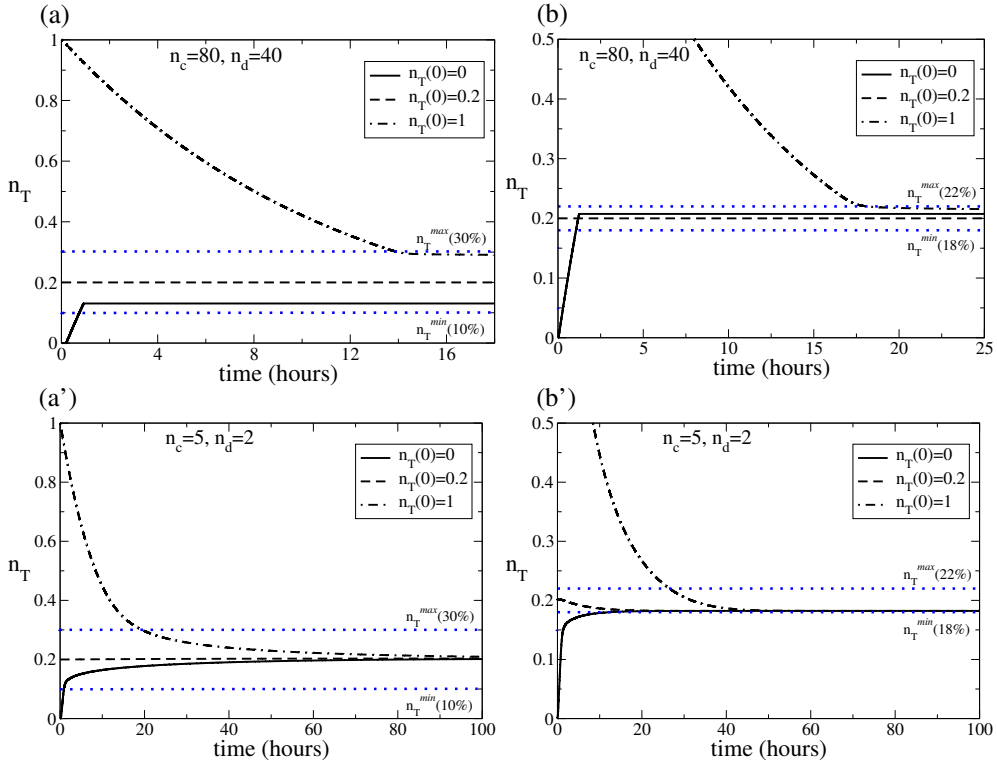


Figure 7: The proportion $n_T$ of PST cells, as a function of time, for different initial conditions $n_T(0)$. Panels (a),(a'): $n_T^{max} = 0.3$, $n_T^{min} = 0.1$ (dotted blue lines). In this case, the parameters are: $a_0 = 39$ nM, $b_0 = 10$ nM, $b_1 = 20$ nM, $a_1 = 77$ nM, $p_1 = 0.52$ nM h$^{-1}$, $d_1 = 0.12$ h$^{-1}$, $p_2 = 3.0$ nM h$^{-1}$, $d_2 = 0.017$ h$^{-1}$. Initial conditions for the chemical signals: $v_c(0) = 60$ nM and $v_D(0) = 30$ nM. Panels (b), (b'): $n_T^{max} = 0.22$ and $n_T^{min} = 0.18$ (dotted blue lines). In this case, the parameters are: $a_0 = 13$ nM, $b_0 = 10$ nM, $b_1 = 20$ nM, $a_1 = 26$ nM, $p_1 = 0.34$ nM h$^{-1}$, $d_1 = 0.12$ h$^{-1}$, $p_2 = 1.6$ nM h$^{-1}$ and $d_2 = 0.017$ h$^{-1}$. Initial conditions for chemical signals are: $v_c(0) = 24$ nM and $v_D(0) = 12$ nM. In all cases, $k_1 = 0.58$ h$^{-1}$, $k_2 = 0.26$ h$^{-1}$, and $U_T + U_P = 1000$.

Finally, because in [9] the authors observed that larger *Dictyostelium* slugs are characterised by lower prestalk proportions, in Fig. 8 we investigate numerically the time-evolution of $n_T$, as we vary the total size of the slug: $U = U_T + U_P$. Here, we consider only the case $n_T^{min} = 0.1$ and $n_T^{max} = 0.3$. The case $n_T^{min} = 0.18$ and $n_T^{max} = 0.22$ leads to similar

results. Figs. 8(a),(b) are obtained with initial conditions $n_T(0) = 0$ (i.e., only PSP cells), while Figs. 8(a'),(b') are obtained with initial conditions $n_T(0) = 1$ (i.e., only PST cells). Overall, the simulations show that for large $n_c$ and $n_d$ values, the final PST proportions depend on the history of the system and on the total cell density $U$. For example, if we start with $n_T(0) = 0$ (as in panel (a)), then the values of $n_T(\infty)$ decrease as we increase $U$. In contrast, if we start with $n_T(0) = 1$ (as in panel (a')), then the values of $n_T(\infty)$ increase as we increase $U$. For small $n_c$ and $n_d$ (see panels (b),(b')), the solution always converges to $n_T(\infty) = 0.2$ (for any initial conditions $n_T(0)$ and any population sizes $U$).

**Remark 1.** *We emphasise here that, while very large values of $n_c$ and $n_d$ do not have a biological meaning, mathematically they lead to step-like functions that can describe phenomenologically the abrupt changes in dynamics observed experimentally [30]. Similar assumptions of step-like functions have been made in [25].*

**Remark 2.** *Throughout this article, we use Hill-type functions to describe the saturated effects of DIF and cAMP concentrations on the PSP↔PST transitions. This particular choice for the transition functions was based on experimental studies that calculated the half-maximum concentration of these two chemicals necessary to induce or inhibit cell differentiation [28, 30, 32]. However, other studies used different types of transition functions. For example, Ràfols et al. [27] ignored cAMP and used transition functions that depended only on DIF: $g_1(v_D) = v_D - u_2$ for $v_D > u_2$ and zero otherwise, and $g_2(v_D) = u_1 - v_D$ for $v_D < u_1$ and zero otherwise. Parameters $u_1$ and $u_2$ are some threshold values for the concentration of DIF. Pate and Othmer [25] also ignored one of the two chemicals, and assumed unrealistic constant transition functions: $g_1(v) = s_1$, $g_2(v) = 0$ for $v > u^*$, and $g_1(v) = 0$, $g_2(v) = s_2$ for $v < u^*$. Here $s_1$ and $s_2$ are the transdifferentiation rates, and $u^*$ is the threshold value for the chemical $v$ that induces the transdifferentiation.*

*Summary of results for the non-spatial model.* In this Section, we developed a realistic non-spatial model that captures the kinetic behaviour of PSP and PST cell transdifferentiation. We showed that (i) the steepness of the Hill transition function and (ii) the initial conditions of the model determine the final cell-type proportions in *Dictyostelium* slugs.

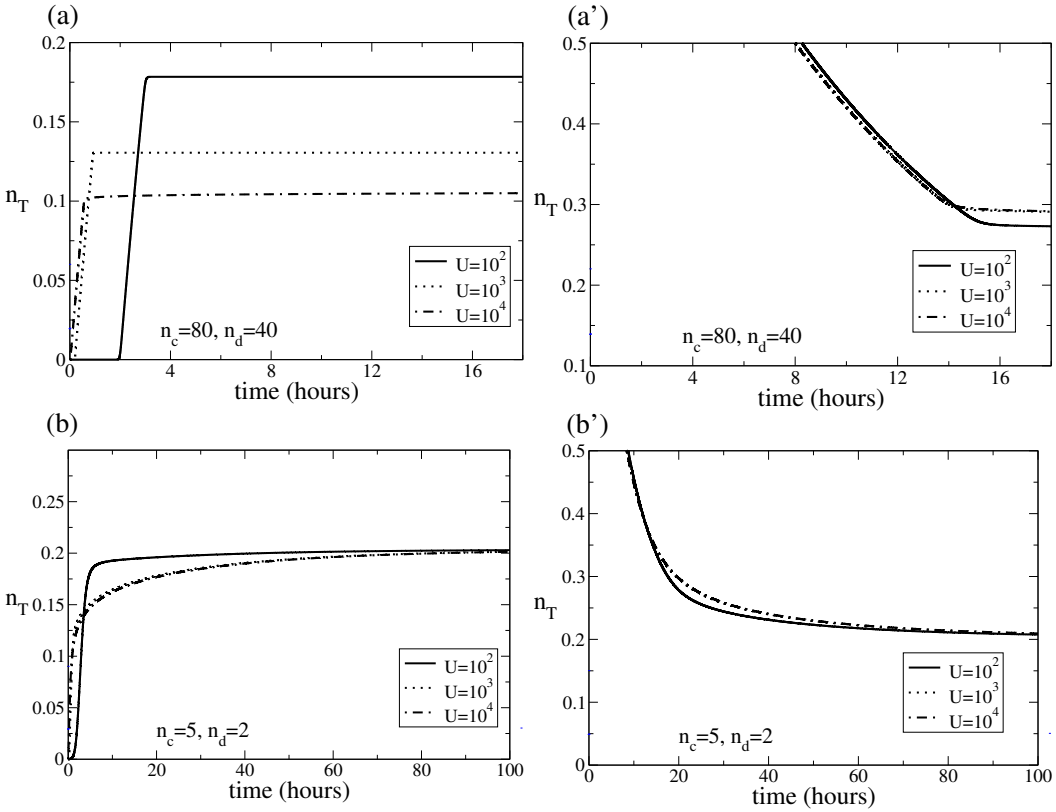


Figure 8: Time series of $n_T$ for different cell numbers $U = U_T + U_P$. Here, $n_T^{max} = 0.3$ and $n_T^{min} = 0.1$. Top panels: $n_c = 80$ and $n_d = 40$. Bottom panels: $n_c = 5$ and $n_d = 2$. Finally, left panels start with $U_T(0) = 0$ and right panels with $U_T(0) = 1$. The parameters are: $a_0 = 39$ nM, $b_0 = 10$ nM, $b_1 = 20$ nM, and $a_1 = 77$ nM, $p_1 = 0.52$ nM h$^{-1}$, $d_1 = 0.12$ h$^{-1}$, $p_2 = 3.0$ nM h$^{-1}$, $d_2 = 0.017$ h$^{-1}$, $k_1 = 0.58$ h$^{-1}$, $k_2 = 0.26$ h$^{-1}$. Initial conditions for the chemical signals are: $v_c(0) = 60$ nM and $v_D(0) = 30$ nM.

To keep the model simple (to be able to investigate it in terms of steady states), we ignored here the production of cAMP that naturally occurs in an oscillatory manner. However, this is an important aspect in spatial models, since it leads to the propagation of excitations waves of cAMP throughout the aggregations of *Dictyostelium* cells. We also did not investigate the spatial sorting of cells as a result of cAMP gradients, which can be observed in slugs or tipped mounds. We address these issues in the next section, where we introduce a spatial model.

## 4. Spatial model

In *Dictyostelium discoideum*, complex cell movement is the result of chemotaxis towards waves of cAMP, as well as mechanical interaction between cells. The aim of this section is to introduce a spatial model that can be used to investigate the role of DIF and cAMP signalling pathways on cell-cell interactions that leads to cell movement, cell sorting and cell proportions in *Dictyostelium discoideum* stationary and moving aggregations.

### *4.1. Model description*

*Dictyostelium* aggregates are 3D structures. However, for simplicity, we assume that our spatial domain is 1D, and the *Dictyostelium* cells can move either left (+) or right (−). We thus denote by $u_P^{\pm}(t,x)$ and $u_T^{\pm}(t,x)$ the number of PSP and PST cells at position $x$ and time $t$. Throughout the rest of the article, we assume that the PSP and PST cells move at averaged constant speeds $\gamma_P$ and $\gamma_T$, and they change their movement directions upon mechanical interactions with other cells and by following cAMP gradients ($v_c$) [21, 34, 35, 36]. Based on experimental data we assume that PST cells are faster compared with PSP cells, ($\gamma_T > \gamma_P$) [5, 8]. However, the case of equal speeds will be also considered for some particular situations. The spatial model for cell movement is described by the following equations [34]:

$$\frac{\partial u_P^+}{\partial t} + \gamma_P \frac{\partial u_P^+}{\partial x} = -\lambda_P^+[v_c; u_P^{\pm}, u_T^{\pm}]u_P^+ + \lambda_P^-[v_c; u_P^{\pm}, u_T^{\pm}]u_P^- + 0.5F, \tag{10a}$$

$$\frac{\partial u_P^-}{\partial t} - \gamma_P \frac{\partial u_P^-}{\partial x} = +\lambda_P^+[v_c; u_P^{\pm}, u_T^{\pm}]u_P^+ - \lambda_P^-[v_c; u_P^{\pm}, u_T^{\pm}]u_P^- + 0.5F, \tag{10b}$$

$$\frac{\partial u_T^+}{\partial t} + \gamma_T \frac{\partial u_T^+}{\partial x} = -\lambda_T^+[v_c; u_P^{\pm}, u_T^{\pm}]u_T^+ + \lambda_T^-[v_c; u_P^{\pm}, u_T^{\pm}]u_T^- - 0.5F, \tag{10c}$$

$$\frac{\partial u_T^-}{\partial t} - \gamma_T \frac{\partial u_T^-}{\partial x} = +\lambda_T^+[v_c; u_P^{\pm}, u_T^{\pm}]u_T^+ - \lambda_T^-[v_c; u_P^{\pm}, u_T^{\pm}]u_T^- - 0.5F. \tag{10d}$$

Here, function F describes the transitions between both types of cells as defined by the rigth-hand-sides of Eqs. 1 and Fig. 2:

$$F = -k_1 f_2(v_c) g_1(v_D) u_P + k_2 g_2(v_D) f_1(v_c) u_T, \tag{11}$$

where $u_P = u_P^+ + u_P^-$ and $u_T = u_T^+ + u_T^-$. (Note the connection between the cell densities in (10) and the cell densities in (1): $U_{P,T} = \int_D u_{P,T}(x,t)dx$, with

$D$ the spatial domain.) The symbols $\lambda^{+}_{P,T}$ ($\lambda^{-}_{P,T}$), denote the turning rates for the cells that were initially moving to the right (left) and then turned to the left (right). These turning rates have a random component that describes the intrinsic randomness of cell motility, as well as a direct component that describes turning in response to cell-cell mechanical interactions (i.e., repulsive and attractive interactions) and turning in response to gradients of cAMP:

$$\lambda^{\pm}_{P} = \lambda^{\pm}_{1P} + \lambda^{\pm}_{2P} f_0(y^{\pm}_{P}), \qquad \lambda^{\pm}_{T} = \lambda^{\pm}_{1T} + \lambda^{\pm}_{2T} f_0(y^{\pm}_{T}). \tag{12}$$

The constants, $\lambda^{\pm}_{1P,1T}$ and $\lambda^{\pm}_{2P,2T}$, represent the random turning rates and the direct turning rates, respectively. We choose $f_0$ to be dimensionless, bounded and increasing functional of the dimensionless functions $y^{\pm}_{P,T}$ that incorporate the mechanical and chemical cell-cell interaction terms:

$$y^{\pm}_{P} = y^{\pm}_{mech,P} + y^{\pm}_{chem,P}, \qquad y^{\pm}_{T} = y^{\pm}_{mech,T} + y^{\pm}_{chem,T}. \tag{13}$$

An example of such function is $f_0(y^{\pm}) = 0.5 + 0.5\tanh(y^{\pm} - y_0)$. The constant $y_0$ is chosen such that in the absence of any mechanical or chemical interactions ($y^{\pm}_{P,T} = 0$), we have $f(0) \ll 1$ and the random turning dominates the movement (see Fig. 9). However, because experimental data shows that the cells in mounds and slugs move continuously with little random motion, in this work we assume small values for these random turning rates [7, 37].

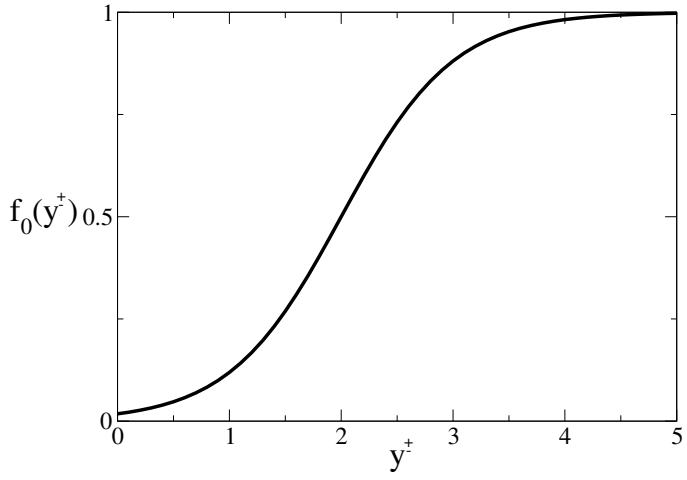


Figure 9: The turning function $f_0(y)$. The constant $y_0 = 2$ shifts the graph to the right such that for $y^{\pm} \approx 0$, the random turning dominates the movement.

To describe cell-cell mechanical interactions, we consider the following nonlocal terms:

$$y^{\pm}_{mech,P} = \pm \int_{-L}^{L} [K_{PT}(s)(u_T(x+s) - u_T(x-s)) + K_{PP}(s)(u_P(x+s) - u_P(x-s))]ds, \tag{14a}$$

$$y^{\pm}_{mech,T} = \pm \int_{-L}^{L} [K_{TP}(s)(u_P(x+s) - u_P(x-s)) + K_{TT}(s)(u_T(x+s) - u_T(x-s))]ds. \tag{14b}$$

These nonlocal terms can model the strong local repulsive interactions between tightly-packed cells, as well as long-range interactions between cells, which occur via the slime sheath that surrounds the slug or via the pulling/pushing of the substratum [38]. The main idea behind these expressions are found in [39]. For instance, a cell positioned at $(x, t)$ interacts with other cells located to its left (at $x - s$) and to its right (at $x + s$), which are within a perception interval $[-L, L]$. Here, kernels $K_{ij}$ are standard Morse-type potentials that describe the balance between the attractive and repulsive interactions between cells:

$$K_{i,j}(s) = -k_a^{i,j} e^{-|s|/s_a} + k_r^{i,j} e^{-|s|/s_r}, \quad i,j = P,T, \quad s \in [-L, L]. \tag{15}$$

Parameters $k_a^{i,j}$ and $k_r^{i,j}$ describe the strength of the interactions, while the constant parameters $s_a$ and $s_r$ describe the length scale of the interactions. Figure 10 shows a plot of this kernel.

*Dictyostelium* cells show direct motion response towards increasing cAMP concentrations [36]. Thus, the dependence of the turning rates on gradients of cAMP is expressed as:

$$y^{\pm}_{chem,P} = \mp \beta_P \nabla v_c, \quad y^{\pm}_{chem,T} = \mp \beta_T \nabla v_c, \tag{16}$$

where $\beta_P$ and $\beta_T$ are the chemotactic sensitivities of PSP and PST cells, respectively. The terms $y^{\pm}_{chem,P,T}$ are also dimensionless.

The cAMP signalling is described by the Martiel and Goldbeter (MG) mechanism [40] for cAMP kinetics. This mechanism describes excitable behaviour (i.e., amplification of supra-threshold pulses), adaptation to constant stimuli and autonomous oscillations. It incorporates the following processes for signal relaying by cells. Cells have a transmembrane cAMP receptor

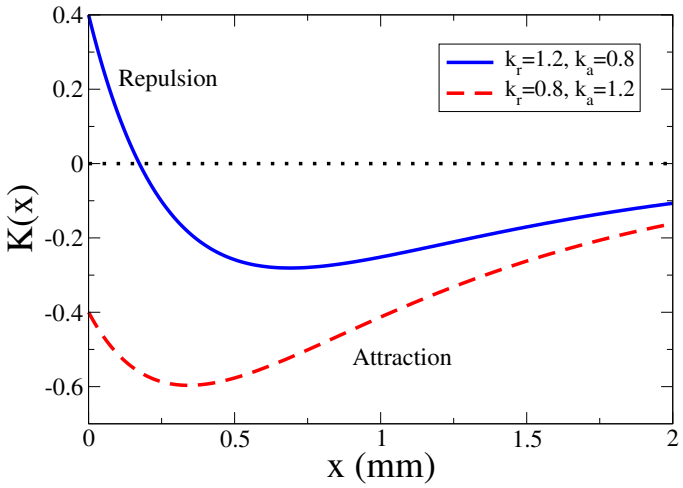


Figure 10: The Morse kernel (15), for attractive-repulsive interactions between cells, for $s_a = 1.0$ mm, $s_r = 0.3$ mm. The blue continuous curve is obtained for $k_r = 1.2$ mm$^{-1}$, $k_a = 0.8$ mm$^{-1}$. The red dashed curve is obtained for $k_r = 0.8$ mm$^{-1}$, $k_a = 1.2$ mm$^{-1}$. The maximum range of interactions is determined by the parameter $L$ that appears in the nonlocal mechanical interaction terms (14). We assume here that cells can sense other cell further away that push/pull the substrate (or produce the slime sheath), and thus $L$ has the length of the whole aggregation.

which can be in either of two states: active or inactive. In the active state, the receptor can bind external cAMP, thereby stimulating the synthesis of cAMP inside the cell. This internal cAMP is transported to the outside of the cell, where it stimulates the cAMP receptor and thereby closes the positive feedback loop. The cAMP receptor changes to the inactive state as a result of prolonged exposure to high external cAMP concentrations. This limits the cAMP production and makes the cell refractory. Meanwhile, the external cAMP decays. In the original mathematical model for this mechanism [40], there were three variables that described the change of extracellular cAMP, intracellular cAMP and the activation state of the cAMP receptors. For computational simplicity, here we use a minimal model consisting of a set of two coupled partial differential equations. This simpler model, which nevertheless retains the important biochemical characteristics of the three-equation model [14, 40, 41], describes the time-evolution of external cAMP

and the state of the cAMP receptor as follows:

$$\frac{\partial V_c}{\partial t} = h(u) - k(u)V_c + D_c\frac{\partial^2 V_c}{\partial x^2}, \tag{17a}$$

$$\frac{dV_r}{dt} = -f_{1r}(V_c)V_r + f_{2r}(V_c)(1 - V_r). \tag{17b}$$

The first equation describes the change in the normalised concentration $V_c$ of extracellular cAMP. This quantity is related to the concentration $v_c$ of external cAMP produced by all cells, through the relation $v_c = K_R V_c$, where $K_R = 100nM$ is the dissociation constant of the phosphorylated receptor complexes [40]. The terms $h(u)$ and $k(u)$ describe the dependence of the production and decay of cAMP on the total cell density, $u = u_P + u_T$. Although *Dictyostelium* aggregates are heterogeneous excitable media with likely differences between the excitability of PST and PSP cells, for simplicity in this study we consider only the case of equal excitability. Thus, as in [40], we assume that:

$$h(u) = q'\sigma\phi(V_c, v_r)u, \quad k(u) = k_e u, \tag{18}$$

where

$$q^{'} = \frac{qk_t}{h(k_i + k_t)}, \quad \phi(V_c, v_r) = \frac{\lambda_1 + Y^2}{\lambda_2 + Y^2}, \quad Y = \frac{V_r V_c}{1 + V_c}. \tag{19}$$

Cells are coupled by diffusion of the extracellular cAMP. Therefore, we include in (17a) a diffusion term, with $D_c$ denoting the diffusion coefficient of cAMP [41]. The parameters that appear in equations (18)-(19) are described in more detail in [40], and their values are given in Table B.2.

Equation (17b) defines the time-evolution of the fraction $V_r$ of active receptors per cell. As in [40], the terms that appear in this equation are:

$$f_{1r}(V_c) = \frac{k_1^{'} + k_2^{'}V_c}{1 + V_c}, \quad f_{2r}(V_c) = \frac{k_{-1}^{'} + k_{-2}^{'}cV_c}{1 + cV_c}. \tag{20}$$

Note that the cells densities do not enter the equation for the receptors, since this equation is written in terms of the fraction of active receptors per cell [14]. However, as receptors are convected with cells, a convention term should be added to Eq. (17b). This term turns out to be very small for the case analysed in this work, as the cAMP wave speed is likely much greater than cell velocity, and therefore we neglect it here [14]. Again, the parameters that appear in Eqs. (17b)-(20) are described in more detail in [40, 41], and their values are given in Table B.2.

We now proceed with the coupling of Eqs. (17) and (10) through Eq. (16). We note that experiments show that cells move only in the cAMP wavefront and remain more or less stationary in the back of the wave. As it stands, Eq. (16) would predict cell movement both in wavefont and waveback. This would lead to a small net translocation opposite to the direction of wave propagation. Thus, the chemotactic cell response cannot solely be determined by the local cAMP gradient [7, 14]. It is well-known that the chemotactic machinery of a cell exhibits desensitisation upon exposure to cAMP. When the wave passes and the concentration falls, cells are desensitised and as result do not turn round to follow the passing wave. Here, we account for this threshold response of the cell to the cAMP gradient by a sigmoid relation between the chemotactic coefficients $\beta_{P,T}$ (which appear in Eq. (16)) and the fraction of active receptors $V_r$ (which is a desensitising component of the chemotactic pathway [40]):

$$\beta_P = \beta_{P0}\frac{V_r^m}{A^m + V_r^m}, \quad \beta_T = \beta_{T0}\frac{V_r^m}{A^m + V_r^m}, \quad m > 1, \tag{21}$$

where $A$ is a positive constant sensing threshold. The parameters $\beta_{P0}$ and $\beta_{T0}$ are the chemotactic intensities of PSP and PST cells, respectively. In this case we can distinguish between the wave front, where cells accelerate in response to the chemotactic signal, from the wave back, where cells desensitised and do not respond to the cAMP gradient.

Finally, the equation for the spatial diffusion of DIF is

$$\frac{\partial v_D}{\partial t} = p_1 u_P - d_1 v_D u_T + D_d \frac{\partial^2 v_D}{\partial x^2}, \tag{22}$$

where $p_1$ describes the production rate of DIF by prespore cells and $d_1 v_D$ is the decay rate of DIF in the presence of prestalk cells. The parameter $D_c$, denotes the diffusion coefficient of DIF [42].

### *4.2. Numerical Results*

Next, we discuss the dynamics of model (10) in two cases: (i) when the PST region is removed, leaving only the PSP cells to form a mound; (ii) when the PSP region is removed, leaving only the PST cells to form a slug. Since the two behaviours occur for different parameter values, we will discuss them separately.

For the numerical simulations, we discretise model (10) on an 1D dimensional domain of length 10 mm ($D = [0, 10]$), and assume periodic boundary

conditions. The numerical integration adopts a time splitting method, which calculates first the time propagation of the reaction part, and then the time propagation of the advection and diffusion parts. Equations are first discretised in space on a uniform mesh (with space step $\Delta x = 10^{-2}$ mm), and the system is then integrated in time with a time step $\Delta t = 10^{-3}$ min. Integration of the reaction terms is performed with a fourth-order Runge-Kutta method. The diffusion term is integrated using a Crank-Nicholson method (with periodic boundary conditions), while the advective term is integrated using the upwind/downwind scheme (also with periodic boundary condition). The nonlocal attraction-repulsion terms are approximated using Simpson's method (with periodic boundary conditions that see the nonlocal terms being wrapped around the domain). The numerical codes were written in Fortran 90.

(i) *Cell sorting and cell-type conversion in isolated PSP fragments*
Many studies show that after removal of the slug tip (i.e., the PST domain), the isolated PSP domain may form a mound that cannot keep migrating, but exhibits transdifferentiation from PSP to PST until a new tipped mound and a slug are formed [9, 12, 13]. The cells differentiate at random positions, and then undergo chemotactic cell sorting. In this section, we use our 1D model (10) to perform qualitative simulations for the proportion regulation process and cell sorting process occurring in this initial stage of *Dictyostelium* development. However, before discussing the results of numerical simulations, we need to discuss the assumptions we make here in regard to the two chemicals, DIF and cAMP.
DIF is a diffusible chemical, and the PSP cells that produce it are initially randomly distributed throughout the whole mound (so it is likely that all cells experience similar DIF concentrations at this stage of development). Moreover, since the PSP cells move inside the mound leading to a distribution of DIF throughout the whole aggregation [4, 42], we decided to keep the model simple and ignore any DIF gradients for now. This suggests that we may consider a homogeneous spatial distribution of DIF concentration governed by

$$\frac{dv_D}{dt} = p_1 U_P - d_1 v_D U_T, \tag{23}$$

with $U_P = \int_D u_P(s)ds$ and $U_T = \int_D u_T(s)ds$ the total number of PSP and PST cells forming the mound, respectively. Under these idealised

conditions, the mound constitutes a group of cells globally coupled through the homogenous distribution of DIF (here, $v_D$ is the concentration of DIF perceived by all cells at a time). Previous theoretical works also assumed a global coupling mechanism to analyse cell type proportioning in homogeneous environments [26, 43, 44].

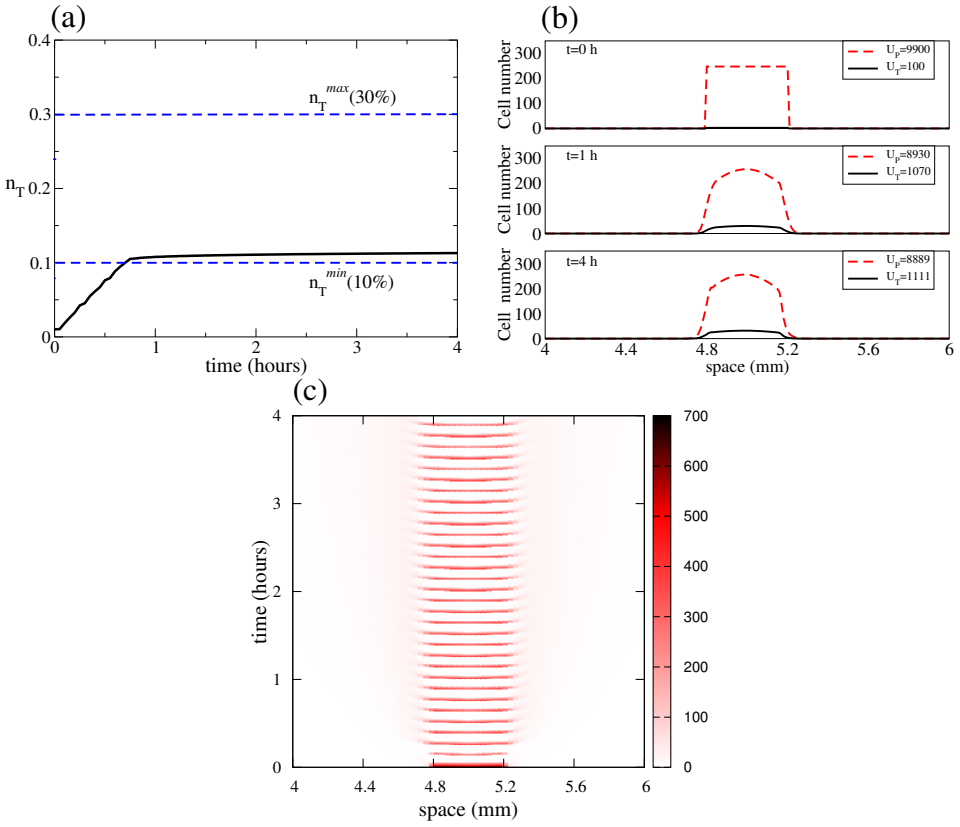


Figure 11: 1D simulations of a mound-like aggregate. Initially, $U_P(0) = 9900$, $U_T(0) = 100$ (with the right-moving cells $U_T^+(0) = 50$, $U_P^+(0) = 4950$, and the left-moving cells $U_T^-(0) = 50$, $U_P^-(0) = 4950$). The cells are homogeneously distributed in a 0.4 mm domain. (a) Temporal evolution of PST proportion, $n_T$. (b) Spatial distribution of cells for $t = 0$, 1, and 4 hours. (c) Evolution of cAMP concentration through the aggregate. For chemicals, $v_D(0) = 30$ nM, $v_c(0) = 2.5$ nM, and $v_r(0) = 0.8$ nM through the whole aggregate. Parameters for cell transdifferentiation and cell motility as in Table B.3 and B.4, respectively. In all cases, $n_T^{\max} = 0.3$ and $n_T^{\min} = 0.1$. These limits are represented in panel (a) by the blue dashed lines. The values of the speeds are: $\gamma_T = \gamma_P = 0.003$ mm/min.

The dynamics of cAMP is much more complex, because the mound is

an excitable medium characterised by the propagation (as expanding concentric rings or spirals) of cAMP waves [5]. The cAMP signal relaying mechanism is local: the extracellular cAMP diffuses through the mound, while cells respond to local increases in cAMP concentration by synthesising more cAMP and excreting it. This process is repeating by the following neighbour cells, leading to the propagation of waves through the mound. Therefore, Eqs. (17) are used to model cAMP signalling. Experimental observations show that under the influence of these cAMP waves, cell motility is slow and towards the organising centre [5]. For our numerical simulations, we assume that cAMP propagation is initiated by periodical stimulation of the cells located in the centre of aggregate.

In Fig. 11, we focus on the case where $n_T(\infty) \in [0.1, 0.3]$ (as it happens for $n_c = 40$ and $n_d = 18$). We also assume that the motility properties of both types of cells are identical (i.e., cell movement speed, mutual mechanical interactions, and chemotactive sensitivities; see Table B.4). Figure 11(a) presents the evolution in time of PST proportion, $n_T$. Initially, there is a massive transdifferentiation from PSP to PST. Then, after $n_T$ crosses the lower threshold $n_T^{min} = 0.1$, the rate of cell differentiation decreases and eventually stops. The corresponding configurations of cells, for $t = 0$, 1, and 4 hours, is presented in Fig. 11(b). Cells end up being distributed around the centre of the aggregation (where we positioned the pacemaker), with a PST proportion of $n_T \approx 0.11 \in [0.1, 0.3]$. A typical spatiotemporal evolution of cAMP concentration is plotted in Fig. 11(c). One can observe the cAMP pulses propagating from the centre, with a period of approximately 7.5 minutes.

In reality, PSP and PST cells differ in many aspects: PST cells are faster (stronger chemotactic forces), more excitable (produce more cAMP), and less adhesive (lower viscosity) [17, 20]. This led us to investigate the case of different speeds, chemotactic sensitivities, and mechanical interactions. In particular, we assume the extreme case in which cell-cell interactions between PST cells and between PST cells and PSP cells are zero ($K_{TT} = K_{TP} = 0$). Then, the direct turning rates for the PST cells will only depend on the chemotactic interaction with cAMP gradients ($Y_T^{\pm} = y_{chem,T}^{\pm}$). It is also reasonable to assume very small random turning rates for the PST cells (see Table B.4). In addition, we assume that $\beta_{T0} > \beta_{P0}$ and $\gamma_T > \gamma_P$.

Figure 12(b) shows the sorting of the faster and newly differentiated

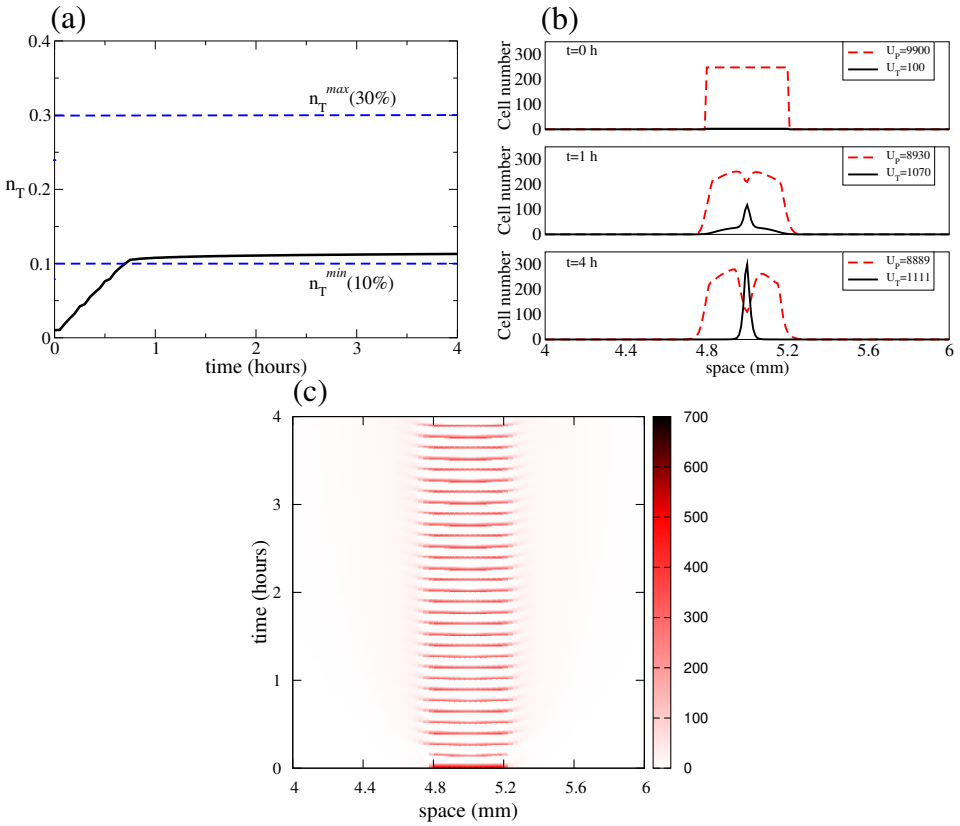


Figure 12: 1D analogy of a tipped-mound aggregate. Initially, $U_P(0) = 9900$, $U_T(0) = 100$ (with the right-moving cells $U_T^+(0) = 50$, $U_P^+(0) = 4950$, and the left-moving cells $U_T^-(0) = 50$, $U_P^-(0) = 4950$). The cells are homogeneously distributed in a 0.4 mm domain. (a) Temporal evolution of PST proportion, $n_T$. (b) Spatial distribution of cells for $t = 0$, 1, and 4 hours. (c) Evolution of cAMP concentration through the aggregate. For chemicals, $v_D(0) = 30$ nM, $v_c(0) = 2.5$ nM, and $v_r(0) = 0.8$ nM through the whole aggregate. Parameters for cell transdifferentiation and cell motility are shown in Tables B.3 and B.4, respectively. In all cases, $n_T^{\max} = 0.3$ and $n_T^{\min} = 0.1$. These limits are represented by the blue dashed lines in (a). The values of the speeds are: $\gamma_T = 0.006$ mm/min and $\gamma_P = 0.003$ mm/min (note the difference from the speeds used in Figure 11).

PST cells to the middle of the aggregation (at $t = 0$, $t = 1$, and $t = 4$ hours). This behaviour is a clear 1D analogy to the 3D tipped mound situation. Initial conditions are as in Fig. 11. Figure 12(a) shows the evolution in time of PST proportion, $n_T$. As before, there is a massive transdifferentiation from PSP to PST. Then, after $n_T$ crosses the lower

threshold, $n_T^{min} = 0.1$, the rate of cell conversion decreases and eventually stops. A typical spatiotemporal evolution of cAMP concentration is plotted in Fig. 12(c). Pulses propagate from the centre of the aggregation (where the pacemaker is).

(ii) *Cell sorting and cell conversion in isolated PST fragments*
When the tip of a slug (i.e., the PST domain) is isolated, it usually keeps migrating as a small slug. This slug progressively elongates and the transdifferentiation from PST to PSP cells leads to the recovery of the PST:PSP proportions [9]. In this subsection, we use our model to analyse qualitatively this situation.
For migrating *Dictyostelium* slugs, the PST region acts as a pacemaker for cAMP waves. Those waves propagate from the middle of the PST zone to the back of the slug and coordinate the periodic forward movement of cells [7]. However, some earlier studies suggest that the more active anterior PST cells pull the posterior cells through mechanical forces [45]. Other studies suggest that anterior-like cells may provide the motive force for the prespore zone, which at the same time pushes the anterior PST cells [38]. For the purpose of our study, we will assume that the anterior PST cells are the source of chemical forces that control the collective cell movement in the slug. The chemotactic propagation of cAMP waves is initiated by periodical stimulation of the cells placed in the most anterior part of the PST region.
For the numerical simulations presented here, we assume the extreme case in which cell-cell interactions between PST cells and between PST cells and PSP cells are zero ($K_{TT} = K_{TP} = 0$). For simplicity, we also assume that DIF is homogeneously distributed along the slug, and its concentration is governed by Eq. (23). This assumption is valid for small slugs. For medium and large slugs, the gradients of DIF may play an important role in cell dynamics [42]. As for isolated PSP fragments, the spatiotemporal dynamics of cAMP is determined by Eqs. (17). Finally, we assume that the PST cells move faster than the PSP cells (see Table B.4).
Figure 13(a) shows that, starting with a configuration of 100% PST cells ($n_T = 1.0$), a transdifferentiation occurs until the solution trajectory crosses the upper threshold, $n_T^{max} = 0.3$. Meanwhile, the slower and newly formed PSP cells are trailing behind to form the PSP region of slug. The corresponding spatial configuration of cells is pre-

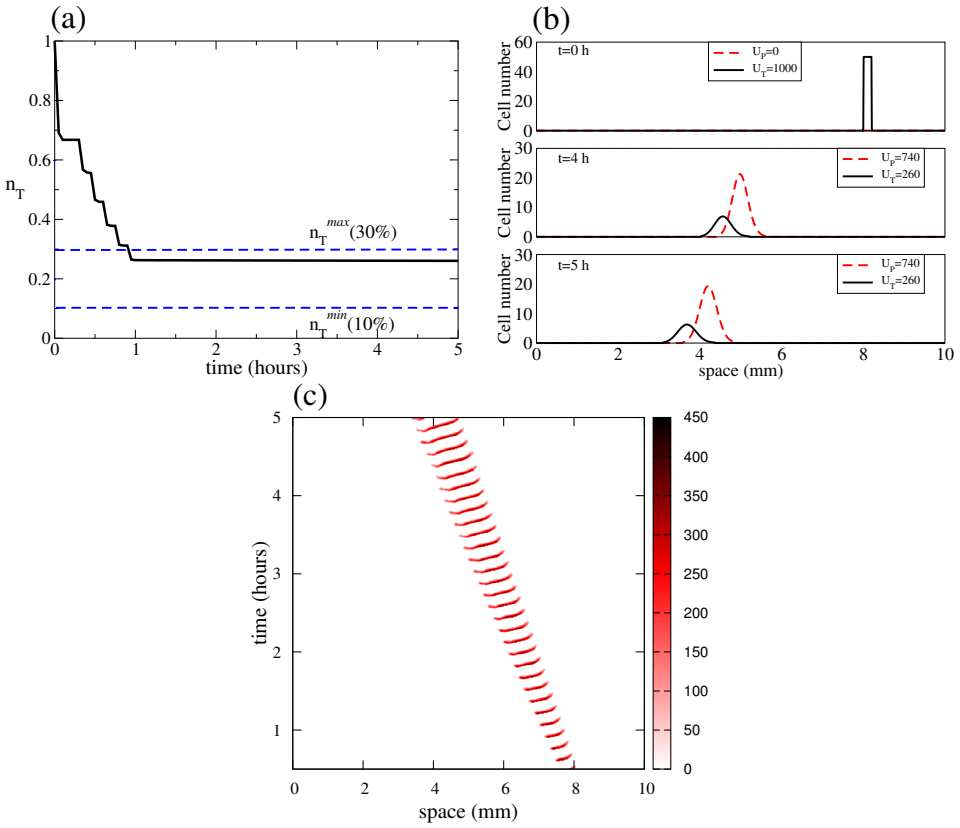


Figure 13: Slug migration and cell differentiation. Initially, $U_P = 0$, $U_T = 1000$ (with the right-moving cells $U_T^+(0) = 500$, $U_P^+(0) = 0$, and the left-moving cells $U_T^-(0) = 500$, $U_P^-(0) = 0$). The PST cells are homogeneously distributed in a 0.2 mm domain. a) Temporal evolution of PST proportion $n_T$. b) Spatial distribution of cells for different times, starting from a configuration of 100% of PST cells (Red dashed line). c) Evolution of cAMP concentration through the slug. Initial data: $v_D(0) = 4.3\ nM$, $v_c(0) = 2.5\ nM$, and $v_r(0) = 0.8\ nM$ through the whole aggregate. Parameters for cell transdifferentiation and cell motility are shown in Tables B.3 and B.4, respectively. In all cases, $n_T^{\max} = 0.3$ and $n_T^{\min} = 0.1$. These limits are represented by the blue dashed lines in (a). The values of the speeds are $\gamma_P = 0.039$ mm/min and $\gamma_T = 0.044$ mm/min.

sented in Figure 13(b). Initially a group of PST cells are distributed homogeneously in a small domain, resembling an isolated PST fragment ($n_T = 1$). A final proportion of $n_T = 0.26$ was established in approximately one hour. Snapshots of a migrating slug conserving the established proportion are shown for $t = 4$ and 5 hours. The spa-

tiotemporal evolution of cAMP concentration is plotted in Fig. 13(c). The slug elongation is reflected by an increase of the excitable medium through which cAMP waves can propagate. The transition rate for the PST $\rightarrow$ PSP differentiation, $k_2$, has been exaggerated (from the value of $k_2 = 0.26$ h$^{-1}$ used in Fig. 7 to the value of $k_2 = 30$ h$^{-1}$) to speed up the formation of the pattern. Note that using a more realistic value of $k_2 = 0.26$ h$^{-1}$ would lead to a stable proportion of PST:PSP cells only after 15h – see Figure 7(a). However, as shown in Fig. 13(b),(c), as time progresses the slug starts to elongate slowly (since we assumed $\gamma_P < \gamma_T$ to match experimental observations). After 15 hours the slug would be unrealistically spread. This issue could be solved by assuming density-dependent velocities $\gamma_{P,T}$ - an approach that will be taken in the future. Finally, we have also verified that in order to get the type of sorting behaviour presented in Fig. 13, cell-cell mechanical interactions are not essential. (However, these interactions are essential to stop the slug elongating even more.)

## 5. Summary and Discussion

In this study, we derived a spatial mathematical model for the dynamics of *Dictyostelium discoideum* cells. We used this model to investigate, in a unitary manner, the role of two cell signalling pathways (via cAMP and DIF morphogens) on cell movement, cell differentiation and cell proportioning inside stationary and moving *Dictyostelium discoideum* aggregations. We started by describing the biological mechanisms (controlled by the cAMP and DIF factors), which we believe are behind cell differentiation. Then, we developed and analysed a non-spatial mathematical model for this mechanism. Finally, we incorporated our cell-differentiation mechanism into a spatial 1D nonlocal hyperbolic model for cell motility. This spatial model allowed us to analyse two specific aggregation cases (i.e., the formation of the mound and the slug), in which the interplay between active cell differentiation and cell sorting plays an important role. To the best of our knowledge, the analysis proposed in this work is one of the first attempts towards a quantitative description of regulation of cell-type proportioning and cell sorting in stationary and moving *Dictyostelium discoideum* aggregations. Some previous attempts have been made in [25] for a model that incorporated only internal sorting and proportionality but not movement of the whole aggregate, or in [23] for models that only consider cell-cell contact as the necessary ingredient

for cell differentiation.

With the help of the non-spatial model, we found that the nature of the final steady state solution is determined by the shape of the transition functions (which are of Hill-type). For very small Hill coefficients, a single steady state solution is achieved, for any initial conditions and system sizes. This situation is in agreement with classical experimental observations in which a perfect regeneration is obtained after the amputation of *Dictyostelium* slugs [13]. However, for large enough Hill coefficients, multiple steady states solutions are possible. Different initial conditions or system sizes lead to different final solutions (i.e., final prestak proportions). This behaviour is consistent with some experimental observations claiming that cell proportions are not exactly restored in slugs after one cell type is removed [9]. However, very large Hill coefficients imply step functions or strict thresholds for cell differentiation. This suggests a discontinuity in cellular behaviour as the thresholds for the morphogens concentrations are crossed. Having these step functions (an approach used previously in [25]) makes sense mathematically, but the functions might not be very realistic from a biological point of view.

The spatial model (10) incorporated multiple aspects of *Dictyostelium* cell dynamics: cell movement, cell turning in response to cAMP waves and cell-cell interactions (via attractive and repulsive forces), cell differentiation in response to cAMP and DIF morphogens. Using this model, we investigated numerically the dynamics of *Dictyostelium* aggregations following the removal of different parts of the slug: (i) the prestalk region, leaving the prespore cells to aggregate into a mound, and (ii) the prespore region, leaving the prestalk cells to form another slug. For the isolated prespore region (case (i)) we found that when the different cell types have identical motility properties, a homogeneous distribution of prespore and prestalk cells is formed, mimicking the initial stage of a *Dictyostelium discoideum* mound. However, by assuming that the prespore and prestalk cells differ in some of their movement properties, we have shown that it is possible to get sorting of the less adhesive and faster moving (newly-formed) prestalk cells to the centre of the aggregate (thus pushing the prespore cells towards the edge of the aggregate). This behaviour is a 1D analogy of the 3D tipped mound situation observed experimentally [5]. With respect to the isolated prestalk region (case (ii)), we also found transdifferentiation from prestalk to prespore cells, and cell sorting of the slow and newly formed prespore cells to the back of the aggregation.

We have also studied numerically (not shown here) how important is the

interplay between the mechanical and chemical cell-cell interactions on the formation and movement of *Dictyostelium* aggregations. As mentioned at the end of the previous section, we have noticed that the mechanical cell-cell interactions are not essential to obtain cell sorting after the removal of the prespore region in the slug (see Figure 13). However, these mechanical interactions are necessary for the formation and sorting of the mound. In this case, the absence of repulsive-attractive interactions will cause cells to pile up around the position of the cAMP pacemaker (see Figure 11). Moreover, for the formation of tipped-mound aggregations, repulsive interactions are essential for the displacement of the PSP cells by the PST cells (see Figure 12).

The above-mentioned behaviours reproduce qualitatively various experimental observations of stationary and travelling *Dictyostelium* aggregations. However, model (10) has some limitations. In reality, Dictyostelium cells do not move at a constant speed. For example, it has been shown that in *Dictyostelium discoideum* aggregations, cells speed depends on the chemoattractant and on its spatial and temporal gradients [17, 20, 34, 35]. The cells also speed-up or slow-down as a consequence of cell-cell mechanical interactions or interactions with the substratum and the so-called slime sheath that surrounds the slug [38]. In the absence of the PST region, the constant speeds $\gamma_P$ make the PSP cells to move either left or right (not shown here). This movement will lead to the spread of cells over the whole domain (since the PSP cells are not kept together anymore by the cAMP - which is produced in the PST region). To address this unrealistic behaviour of PSP cells, in a future study we plan to generalise model (10) to include density- and chemical-dependent speeds. Other possible research directions suggested by this study revolve around the heterogeneity of the *Dictyostelium discoideum* aggregations. In particular, different cells might have different excitability levels. Also, the concentration of DIF is not homogeneous throughout the aggregations, being produced differently by different types of cells (i.e., the prespore cells that produce DIF are positioned at the back of the slug, creating a DIF gradient throughout the slug). Finally, a more realistic model would incorporate 2D or even 3D cell-cell and cell-morphogen interactions.

## 6. Acknowledgments

C.J.W. acknowledges support from the Wellcome Trust grant 094131/Z/10/Z. R.E. acknowledges support from an Engineering and Physical Science Re-

search Council (UK) First Grant number EP/K033689/1.

## Appendix A. Saturation functions that lead to different PST proportions

In Figure 3, we considered $n_T^{max} = 0.3$ and $n_T^{min} = 0.1$ (which, via (9) lead to some specific values of $a_0$ and $a_1$ – after fixing $b_0$, $b_1$ values). In Figure A.14 we show the shape of the saturation functions $f_{1,2}$ and $g_{1,2}$ for $n_T^{max} = 0.22$ and $n_T^{min} = 0.18$ (which lead to different $a_0$ and $a_1$ values, and implicitly to different saturation functions).

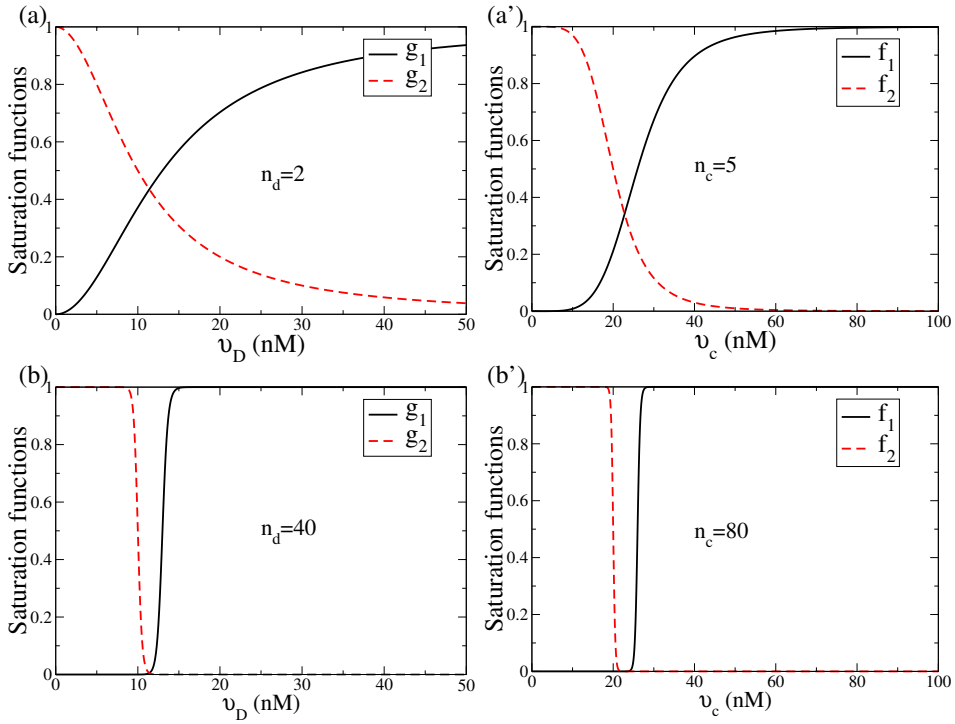


Figure A.14: Examples of saturation functions (2) for $n_T^{max} = 0.22$ and $n_T^{min} = 0.18$ and different values of the exponent coefficients: (a)-(a') $n_d = 2, n_c = 5$ and (b)-(b') $n_d = 40, n_c = 80$. Left panels show saturation functions $g_1(v_D)$ and $g_2(v_D)$. Right panels show saturation functions $f_1(v_c)$ and $f_2(v_c)$. Half maxima concentrations for the saturation functions are $a_0 = 13$ nM, $b_0 = 10$ nM, $b_1 = 20$ nM, and $a_1 = 26$ nM.

## Appendix B. Model parameters

Tables B.1–B.4 show a summary of the variables and parameters that appear in models (1)-(10).

Table B.1: Variables used throughout this article

| Variable | Description |
|---|---|
| $U_P$ | Total number of prespore cells in the aggregate |
| $U_T$ | Total number of perstalk cells in the aggregate |
| $U = U_T + U_P$ | Total number of cells in the aggregate |
| $U_P^+$ | Total number of right-moving prespore cells in the aggregate |
| $U_P^-$ | Total number of left-moving prespore cells in the aggregate |
| $U_T^+$ | Total number of right-moving prestalk cells in the aggregate |
| $U_T^-$ | Total number of left-moving prestalk cells in the aggregate |
| $u_P^-$ | Number of left-moving prespore cells at a position $x \in D$ |
| $u_T^-$ | Number of left-moving prestalk cells at a position $x \in D$ |
| $u_P^+$ | Number of right-moving prespore cells at a position $x \in D$ |
| $u_T^+$ | Number of right-moving prestalk cells at a position $x \in D$ |
| $u_P = u_P^- + u_P^+$ | Total number of prespore cells at a position $x \in D$ |
| $u_T = u_T^- + u_T^+$ | Total number of prestalk cells at a position $x \in D$ |
| $u = u_P + u_T$ | Total number of cells at a position $x \in D$ |
| $v_D$ | Concentration of Differentiation-inducing Factor (DIF) in units of nM |
| $v_c$ | Concentration of extracellular cyclic adenosine-3',5'-monophosphate (cAMP) in units of nM |
| $V_c$ | Normalized concentration of extracellular cAMP |
| $V_r$ | Fraction of receptors in active state |

## Appendix C. Details of some calculations

In this Appendix, we show the details of obtaining Eq. (4) from (3). At steady state Eqs. (1) is reduced to

$$-k_1 g_1(v_D) f_2(v_c) U_P + k_2 g_2(v_D) f_1(v_c) U_T = 0, \tag{C.1a}$$

$$p_1 U_P - d_1 v_D U_T = 0, \tag{C.1b}$$

$$p_2 U_T - d_2 v_c U_P = 0, \tag{C.1c}$$

Table B.2: Martiel-Goldbeter model parameters used throughout this article [40]

| Parameter | Values | Units |
|---|---|---|
| $k_1^{'}$ | 0.036 | $\text{min}^{-1}$ |
| $k_2^{'}$ | 0.666 | $\text{min}^{-1}$ |
| $k_{-1}^{'}$ | 0.36 | $\text{min}^{-1}$ |
| $k_{-2}^{'}$ | 0.0033 | $\text{min}^{-1}$ |
| $k_i$ | 1.7 | $\text{min}^{-1}$ |
| $k_t$ | 5.5 | $\text{min}^{-1}$ |
| $k_e$ | 3.6 | $\text{min}^{-1}$ |
| $h$ | 5 | |
| $q$ | 1000 | $\text{min}^{-1}$ |
| $\lambda_1$ | 0.001 | |
| $\lambda_2$ | 2.4 | |
| $c$ | 10 | |
| $\rho$ | 1 | $\text{min}^{-1}$ |

with $g_1$, $g_2$, $f_1$, and $f_2$ given by Eq. (2) and $n_c = n_d = 1$. Then, after substituting $y = U_P/U_T$ into Eq. (C.1a) and rearranging the terms we get

$$yk_1b_1v_D(b_0 + v_D)(a_1 + v_c) = k_2b_0v_c(b_1 + v_c)(a_0 + v_D). \tag{C.2}$$

From Eqs. (C.1b) and (C.1c) it also follows that

$$v_c = \frac{p_2}{d_2}\frac{1}{y}, \quad v_D = \frac{p_1}{d_1}y. \tag{C.3}$$

Finally, substituting Eq. (C.3) into Eq. (C.2) and re-writting $y = (1 - n_T)/n_T$ with $n_T = U_T/(U_T + U_P)$, we get Eq. (4).

## References


[1] Nanjundiah, V., Saran, S., 1992. The determination of spatial pattern in *Dictyostelium discoideum*. J. Biosci., 17(4), 353-394.

[2] Gross, J.D., 1994. Developmental decisions in *Dictyostelium discoideum*. Microbiol. Rev., 58(3), 330-351.

[3] Weijer, C.J., 2009. The Cellular Basis of *Dictyostelium* Morphogenesis. In S. Nakanishi et al. (eds.), Systems biology: The challenge of Complexity. pp. 209-220.

[4] Kay, R.R., Thompson C.R., 2009. Forming patterns in development without morphogen gradients: scattered differentiation and sorting out. Cold Spring Harb. Perspect. Biol. 1(6), a001503.

[5] Siegert, F., Weijer, C.J., 1995. Spiral and concentric waves organise multicellular *Dictyostelium* mounds. Curr. Biol. 5(8), 937-943.

[6] Weijer, C.J., 2004. *Dictyostelium* morphogenesis. Curr. Opin. Genet. Dev. 14(4), 392-398.

[7] Dormann, D., Weijer. C.J., 2001. Propagating chemoattractant waves coordinate periodic cell movement in *Dictyostelium* slugs. Development, 128(22), 4535-4543.

[8] Siegert, F, Weijer, C.J., 1992. Three-dimensional scroll waves organize *Dictyostelium* slugs. Proc. Nat. Acad. Sci. USA 89(14), 6433-6437.

[9] Ràfols, I., Amagai, A., Maeda, Y., MacWilliams, H.K., Sawada, Y., 2001. Cell type proportioning in *Dictyostelium* slugs: lack of regulation within a 2.5 fold tolerance range. Differentiation, 67(4-5), 107-116.

[10] Maruo, T., Sakamoto, H., Iranfar, N., Fuller, D., Morio, T., Urushihara, H., Tanaka, Y., Maeda, M., Loomis, W.F., 2004. Control of cell type proportion in *Dictyostelium discoideum* by differentiation-inducing factor as determined by in situ hybridization. Eukaryot Cell. 3(5), 1241-1248.

[11] Bonner, J.T., 1957. A theory of the control of differentiation in the cellular slime molds. Quart. Rev. Biol. 32(3), 232-246.

[12] Sakai, Y., 1973. Cell type conversion in isolated prestalk and prespore fragments of the slime mold *Dictyostelium discoideum*. Devl. Growth & Differ. 15, 11-19.

[13] Raper, K.B., 1940. Pseudoplasmodium formation and organization in *Dictyostelium discoideum*. J. Elisha Mitchell Sci. Soc. 56, 241-282.

[14] Hoefer. T., Sherratt, J. A., Maini P.K., 1995. *Dictyostelium discoideum:* cellular self-organization in an excitable biological medium, Proc. R. Soc. London B 259(1356), 249-257.

[15] van Oss, C., Panfilov, A.V., Hogeweg, P., Siegert, F., Weijer, C.J., 1996. Spatial pattern formation during aggregation of the slime mould *Dictyostelium discoideum*. J. Theor. Biol.181(3), 203-213.

[16] Savill, N.J., Hogeweg, P., 1997. Modelling morphogenesis: From single cells to crawling slugs 184(3), 229-235.

[17] Vasiev, B., Weijer, C.J., 1999. Modeling chemotactic cell sorting during *Dictyostelium discoideum* mound formation. Biophys. J. 76(2), 595-605.

[18] Bretschneider, T., Vasiev, B., Weijer., C.J., 1999. A model for cell movement during *Dictyostelium* mound formation. J. Theor. Biol. 189, 41-51.

[19] Marée, A.F.M., Panfilov, A.V., Hogeweg, P., 1999. Migrating and thermotaxis of *Dictyostelium discoideum* slugs, a model study. J. Theor. Biol. 199(3), 297-309.

[20] Bretschneider, T., Vasiev, B., Weijer., C. J., 1999. A model for *Dictyostelium* slug movement. J. Theor. Biol. 199(2), 125-136.

[21] Palsson, E., Othmer, G. H., 2000. A model for individual and collective cell movement in *Dictyostelium discoideum*. Proc. Nat. Acad. Sci. USA 97(19), 10448-10453.

[22] Palsson, E., 2008. A 3-D model used to explore how cell adhesion and stiffness affect cell sorting and movement in multicellular systems. J. Theor. Biol. 254(1), 1-13.

[23] Marée, A.F.M., Hogeweg, P., 2001. How amoeboids self-organise into a fruiting body: multicellular coordination in *Dictyostelium discoideum*. Proc. Nat. Acad. Scie USA 98(7), 3879-3883.

[24] Uchinomia, K., Iwasa, Y., 2013. Evolution of stalk/spore ratio in social amoeba: cell-to-cell interaction via a signalling chemical shaped by cheating risk. J. Theor. Biol., 336, 110-118.

[25] Pate, E.F., Othmer, G.H., 1986. Differentiation, cell sorting and proportion regulation in the slug stage of *Dictyostelium discoideum*. J. Theor. Biol. 118(3), 301-319.

[26] Schaap, P., Tang, Y., Othmer, H.G., 1996. A model for pattern formation in *Dictyostelium discoideum*. Differentiation 60(1), 1-16.

[27] Ràfols, I., MacWilliams, H.K., Maeda, Y., Sawada, Y., 2014. On the conflict between precision and robustness in the proportion regulation of cell types. arXiv:1401.7872.

[28] Kay, R.R., Thompson, C.R., 2001. Cross-induction of cell types in *Dictyostelium*: evidence that DIF-1 is made by prespore cells. Development 128(24), 4959-4966.

[29] Kay, R.R., Flatman, P., Thompson, C.R., 1999. DIF signalling and cell fate. Semin. Cell Dev. Biol. 10(6), 577-585.

[30] Berks, M., Kay, R., 1990. Combinatorial control of cell differentiation by cAMP and DIF-1 during development of *Dictyostelium discoideum*. Development 110(3), 977-984.

[31] Weijer, C.J., Durston, A.J., 1985. Influence of cyclic AMP and hydrolysis products on cell type regulation in *Dictyostelium discoideum*. J. Embryol. Exp. Morphol., 86, 19-37.

[32] Kay, R.R., 1982. cAMP and spore differentiation in *Dictyostelium discoideum*. Proc. Nat. Acad. Sci. USA 79, 3228-3231.

[33] Saran. S., Meima, M.E., Alvarez-Curto, E., Weening, K.E., Rozen, D.E. and Schaap, P., 2002. cAMP signaling in *Dictyostelium*. J. Muscle Research and Cell Motility 23(7-8), 793-802.

[34] Hillen, T., Stevens, A., 2000. Hyperbolic models for chemotaxis in 1-D. Anal. Real World Appl. 1, 409-433.

[35] Soll, D.R., 1990. Behavioral studies into the mechanism of eukaryotic chemotaxis. J. Chem. Ecol. 16(1), 133-150.

[36] Fisher, P.R., Merkl, R., Gerish, G., 1989. Quantitative analysis of cell motility and chemotaxis in *Dictyostelium discoideum* by using an image

processing system and a novel chemotaxis chamber providing stationary chemical gradients. J. Cell. Biol. 108, 973-984.

[37] Rietdorf, J., Siegert, F., Weijer, C.J., 1996. Analysis of optical density wave propagation and cell movement during mound formation in *Dictyostelium discoideum*. Dev. Biol. 177(2), 427-438.

[38] Rieu, J.P., Saito, T., Delanoë-Ayari, H., Sawada, Y., Kay, R.R., 2009. Migration of *Dictyostelium* slug: Anterior-like cells may provide the motive force for the prespore zone. Cell Motil. Cytoskeleton 66(12), 1073-1086.

[39] Eftimie, R., de Vries, G,. Lewis, M.A., Lutscher, F., 2007. Modelling group formation and activity patterns in self-organisation collectives of individuals. Bull. Math. Biol., 69(5), 1537-1565.

[40] Martiel, J.L., Goldbeter, A., 1987. A model based on receptor desensitization for cyclic AMP signalling in *Dictyostelium* cells. Biophys J., 52(5), 807-828.

[41] Tyson, J.J., Alexander, K.A., Manoranjan, V.V, Murray, J.D, 1989. Spiral waves of cyclic AMP in a model of slime mould aggregation. Physica D 34, 193-207.

[42] Brookman, J.J., Jermyn, K.A., Kay, R.R., 1987. Nature and distribution of the morphogen DIF in the *Dictyostelium* slug. Development 100, 119-124.

[43] Nakajima, A., Kaneko, K., 2008. Regulative differentiation as bifurcation of interacting cell population. J. Theor. Biol. 253, 779-787.

[44] Mizuguchi, T., Sano, M., 1995. Proportion regulation of biologically cells in globally coupled nonlinear systems. Phys. Rev. Lett. 75, 966-969.

[45] Inouye, K., Takeuchi, I., 1980. Motive force of the migrating pseudoplasmodium of the cellular slime mould *Dictyostelium discoideum*. J. Cell. Sci. 41, 53-64.

Table B.3: Kinetic parameters for cell transdifferentiation used throughout Section 4.

| Param. | Mound (Fig. 11) | Mound (Fig. 12) | Slug (Fig. 13) | Units | Description |
|---|---|---|---|---|---|
| $n_c$ | 80 | 80 | 80 | - | Hill coefficient controlling the steepness of functions $f_1$ and $f_2$ |
| $n_d$ | 40 | 40 | 40 | - | Hill coefficient controlling the steepness of functions $g_1$ and $g_2$ |
| $k_1$ | 0.58 | 0.58 | 0.58 | $h^{-1}$ | Differentiation rate for prestalk cells |
| $k_2$ | 0.26 | 0.26 | 30 | $h^{-1}$ | Differentiation rate for prespore cells |
| $p_1$ | 0.5 | 0.5 | 0.5 | nM $h^{-1}$ | Rate of DIF production by prespore cells |
| $d_1$ | 0.125 | 0.125 | 0.125 | $h^{-1}$ | Rate of DIF decomposition by prestalk cells |
| $a_0$ | 39 | 39 | 39 | nM | Half-maximal induction of prestalk gene expression |
| $b_0$ | 10 | 10 | 10 | nM | Half-maximal repression of prespore gene expression |
| $a_1$ | 77 | 77 | 77 | nM | Half-maximal induction of prespore gene expression |
| $b_1$ | 20 | 22 | 20 | nM | Half-maximal repression of prestalk gene expression |

Table B.4: Motility parameters for cell movement used throughout Section 4.

| Param. | Mound (Fig. 11) | Mound (Fig. 12) | Slug (Fig. 13) | Units | Description |
|---|---|---|---|---|---|
| $\gamma_p$ | 0.003 | 0.003 | 0.039 | mm $\text{min}^{-1}$ | Speed of prespore cells |
| $\gamma_t$ | 0.003 | 0.006 | 0.044 | mm $\text{min}^{-1}$ | Speed of prestalk cells |
| $\lambda_{1T}^{\pm}$ | 5 | $10^{-5}$ | $10^{-4}$ | $\text{min}^{-1}$ | Random turning rates of prestalk cells |
| $\lambda_{1P}^{\pm}$ | 5 | 5 | $10^{-4}$ | $\text{min}^{-1}$ | Random turning rates of prespore cells |
| $\lambda_{2T}^{+}$ | 5 | 5 | 20 | $\text{min}^{-1}$ | Bias turning rate for right-moving prestalk cells |
| $\lambda_{2T}^{-}$ | 5 | 5 | $10^{-4}$ | $\text{min}^{-1}$ | Bias turning rate for left-moving prestalk cells |
| $\lambda_{2P}^{+}$ | 5 | 5 | 20 | $\text{min}^{-1}$ | Bias turning rate for right-moving prespore cells |
| $\lambda_{2P}^{-}$ | 5 | 5 | $10^{-4}$ | $\text{min}^{-1}$ | Bias turning rate for left-moving prespore cells |
| $y_0$ | 2 | 2 | 2 | - | Shift constant for the turning function |
| $D_c$ | 0.0015 | 0.0015 | 0.0015 | $\text{mm}^2$ $\text{min}^{-1}$ | Diffusion coefficient of cAMP |
| $\beta_{P0}$ | 1 | 1 | 2 | mm $\text{nM}^{-1}$ | Chemotactic sensitivity for prespore cells |
| $\beta_{T0}$ | 1 | 5 | 2 | mm $\text{nM}^{-1}$ | Chemotactic sensitivity for prestalk cells |
| $A$ | 0.77 | 0.77 | 0.77 | - | Response threshold for chemotactic sensitivities |
| $m$ | 10 | 10 | 10 | 10 | Exponent controlling the steepness of the chemotactic coefficients |
| $k_a^{PP}$ | 0.8 | 0.8 | 0.8 | $\text{mm}^{-1}$ | Intensity of attraction between prespore cells |
| $k_a^{PT}$ | 0.8 | 0.8 | 0.8 | $\text{mm}^{-1}$ | Intensity of attraction exerted by prestalk on prespore cells |
| $k_r^{PP}$ | 1.2 | 1.2 | 1.2 | $\text{mm}^{-1}$ | Intensity of repulsion between prespore cells |
| $k_r^{PT}$ | 1.2 | 1.2 | 1.2 | $\text{mm}^{-1}$ | Intensity of repulsion exerted by prestalk on prespore cells |
| $k_a^{TT}$ | 0.8 | 0 | 0 | $\text{mm}^{-1}$ | Intensity of attraction between prestalk cells |
| $k_a^{TP}$ | 0.8 | 0 | 0 | $\text{mm}^{-1}$ | Intensity of attraction exerted by prespore on prestalk cells |
| $k_r^{TT}$ | 1.2 | 0 | 0 | $\text{mm}^{-1}$ | Intensity of repulsion between prestalk cells |
| $k_r^{TP}$ | 1.2 | 0 | 0 | $\text{mm}^{-1}$ | Intensity of repulsion exerted by prespore on prestalk cells |
| $s_a$ | 1 | 1 | 1 | mm | Length scale of attraction |
| $s_r$ | 0.3 | 0.3 | 0.3 | mm | Length scale of repulsion |
| $L$ | 1 | 1 | 1 | mm | Length scale for the perception range |